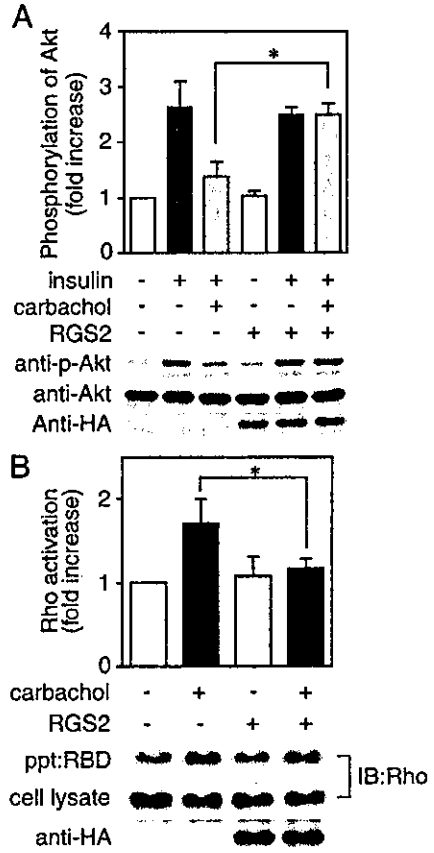

Fig. 7. Effect of RGS2 on the ability of carbachol to inhibit insulin stimulation of Akt and to activate endogenous RhoA. (A) HeLa cells were co-transfected with the m1 receptor, wild type of Akt and HA-tagged RGS2, incubated for 16 h, and starved in DMEM for 2 h. Then the cells were stimulated with insulin, carbachol, or insulin plus carbachol for 5 min, and lysates were immunoblotted with antibodies against phospho-Akt (Ser473), Akt, and HA. The intensity of phospho-Akt (Ser473) band was quantified by densitometry and relative values are shown as means ± SD of data from five experiments (*$P < 0.01$). (B) HeLa cells were co-transfected with the m1 receptor and RGS2, incubated for 16 h, and starved in DMEM for 2 h. Then they were stimulated with carbachol for 5 min. Cell lysates were subjected to the pull-down assay with GST-mDia-RBD, and precipitated RhoA and cell lysates were immunoblotted with the antibodies against RhoA and HA. The intensity of RhoA band in the precipitate was quantified by densitometry and relative values are shown as means ± SD of data from five experiments (*$P < 0.01$).

stimulated the cleavage (Fig. 8A). The expression of the constitutively active mutant of Akt almost completely inhibited the effects of the constitutively active mutants of RhoA or carbachol (Figs. 2 and 8A). Expression of the constitutively active mutant of RhoA, however, did not change insulin-stimulated phosphorylation of Akt (data not shown), suggesting the pathway mediated by RhoA to be different from that through Akt. In support of this hypothesis, carbachol-induced ROCK-I cleavage was partially inhibited by the expression of the dominant-negative mutant of RhoA and the addition of orthovanadate, respectively, and completely inhibited by their combination (Fig. 8B). Similarly, carbachol treatment increased the number of apoptotic cells, and the blockage of tyrosine phosphatase or Rho pathways

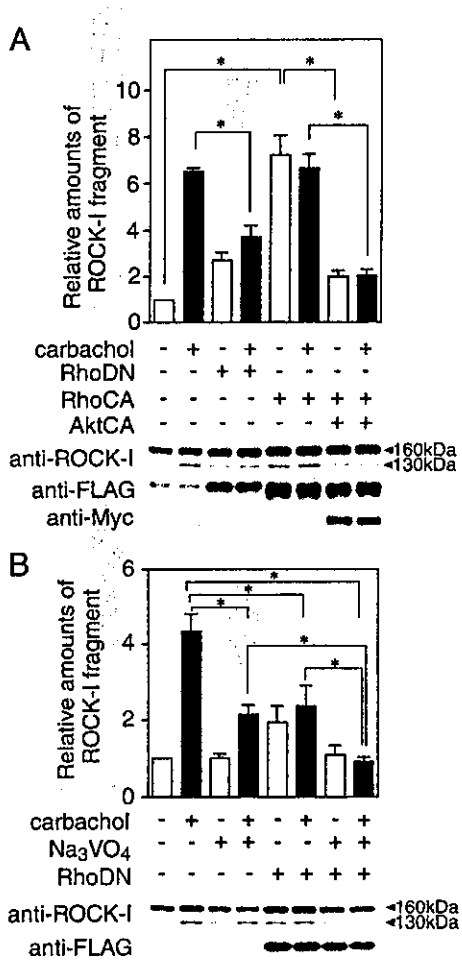

Fig. 8. Effects of RhoA mutants, a constitutively active form of Akt and orthovanadate, and their combination on carbachol induced-ROCK-I cleavage. (A) HeLa cells were co-transfected with the m1 receptor, ROCK-I, a dominant negative mutant of RhoA (RhoDN), a constitutively active mutant of RhoA (RhoCA), and constitutively active mutants of Akt (AktCA), and incubated for 16 h. Then the cells were stimulated with carbachol for 4 h, and lysates were immunoblotted with antibodies against ROCK-I, FLAG, and Myc. The intensity of the 130-kDa band was quantified by densitometry and relative values are shown as means ± SD of data from four experiments (*$P < 0.01$). (B) HeLa cells were co-transfected with the m1 receptor, ROCK-I and the dominant negative mutant of RhoA, and incubated for 16 h. Then the cells were stimulated with carbachol for 4 h, either with or without prior treatment for 1 h with 1 mM orthovanadate, and lysates were immunoblotted with antibodies against ROCK-I and FLAG. The intensity of the 130-kDa band was quantified by densitometry and relative values are shown as means ± SD of data from five experiments (*$P < 0.01$).

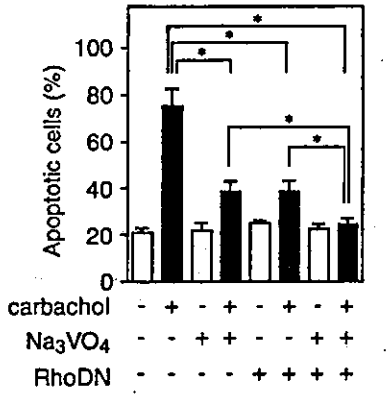

Fig. 9. Effects of orthovanadate and a dominant negative mutant of RhoA and their combination on carbachol-induced apoptosis. HeLa cells were co-transfected with the m1 receptor, GFP and a dominant negative mutant of RhoA, and incubated for 16 h. Then cells were stimulated with carbachol for 4 h, either with or without prior treatment for 1 h with 1 mM orthovanadate. The percentage of apoptotic cells was then assessed as described under Materials and methods. A minimum of 500 cells was counted for each plate under randomized conditions. The results are shown as means ± SD of data from four experiments (*$P < 0.01$).

caused only partial recovery. But the combination of orthovanadate and the dominant negative mutant of RhoA additively and completely inhibited the effect of carbachol (Fig. 9). These results suggested that carbachol induces apoptosis through $G_{q/11}$ via two independent pathways involving protein tyrosine phosphatases and RhoA.

Discussion

In the present study, we investigated the molecular mechanisms of $G_{q/11}$-induced apoptosis in HeLa cells, and found that $G_{q/11}$ signaling activated RhoA and reduced the phosphorylation of Akt stimulated by insulin through tyrosine phosphatase (Fig. 10). The ability of carbachol to inhibit insulin-stimulated Akt phosphorylation was decreased by orthovanadate or pervanadate, indicating the involvement of protein tyrosine phosphatase. Carbachol inhibited insulin-stimulated phosphorylation of IRS-1, and this effect was canceled by orthovanadate, suggesting IRS-1 to be a possible substrate for a $G_{q/11}$-stimulated tyrosine phosphatase. In m1 receptor-transfected HeLa cells, carbachol also inhibited epidermal growth factor-stimulated phosphorylation of Akt, but orthovanadate did not affect the ability of carbachol (data not shown). These observations support the possibility that $G_{q/11}$ stimulates insulin signaling-specific protein tyrosine phosphatases. A recent study showed that $G\alpha_{12}$ and $G\alpha_{13}$ interact with serine–threonine protein phosphatase type 5 and stimulate its phosphatase activity [39]. Therefore, a protein tyrosine phosphatase that interacts with $G\alpha_{q/11}$ and stimulates its phosphatase activity may be present in HeLa cells. However, our attempt to detect G_q-activated protein tyrosine phosphatase activity using a phosphorylated peptide, which had the specific amino acid sequence of IRS-1, as a substrate was unfortunately not successful (data not shown). In contrast, a previous report showed receptor protein tyrosine phosphatase α to be regulated by the m1 receptor via protein kinase C activation [32], suggesting the possibility of an indirect action of $G_{q/11}$.

In addition to tyrosine phosphatase, $G_{q/11}$ signals also activate RhoA to induce apoptosis in HeLa cells. A recent study demonstrated that G_q and m1 stimulation impacts on Rho in HEK293 cells through a pathway independent of the stimulation of protein kinase C and upregulation of intracellular Ca^{2+} [34]. We have previously reported that this is similarly the case with G_{11}-induced apoptosis [8], and have also shown that the inhibition of Akt phosphorylation by carbachol does not involve phospholipase C activation in the present study. Similar observations in HEK293 and HeLa cells suggest the same mechanisms of Rho activation by G_q signals to be operating in both cell lines.

Recent studies demonstrated that $G\alpha_q$ and $G\alpha_{11}$ regulate actin cytoskeleton remodeling through activation of ADP-ribosylation factor 6 in CHO or 3T3-L1 cells [40,41]. However, both constitutively active and dominant negative forms of ADP-ribosylation factor 6 did not alter the effects of carbachol on insulin-stimulated Akt phosphorylation in HeLa cells (data not shown). Progression from hypertrophy to apoptosis was found to be coincident with the activation of c-Jun N-terminus kinase in $G\alpha_q$-overexpressing cardiomyocytes and transgenic mice [3]. However, when we added an inhibitor of c-Jun N-terminus kinase (SP600125), it did not

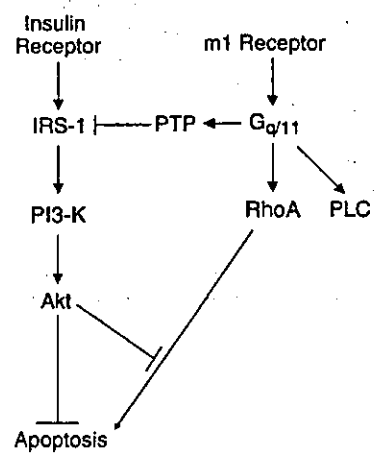

Fig. 10. Schematic overview showing an interpretation of the results of the present study. The m1 receptor stimulates $G_{q/11}$, which leads to the activation of protein tyrosine phosphatases (PTP) and RhoA. Activated PTP then dephosphorylates insulin-stimulated IRS-1 and results in the inhibition of insulin-stimulation of Akt through the phosphoinositide 3-kinase (PI3-K) pathway. The inhibition of insulin-stimulation of Akt induces apoptosis in HeLa cells. Activated RhoA also induces apoptosis through unknown mechanisms and this pathway is inhibited by activated Akt.

block the effect of carbachol on Akt phosphorylation (data not shown).

$G_{q/11}$-induced apoptosis seems to be cell-specific, because m1 receptor stimulation by carbachol and a constitutively active mutant of $G\alpha_{11}$ did not induce apoptosis but rather stimulated the phosphorylation of Akt in NIH3T3 cells (data not shown). Similarly, a previous study showed that $G\alpha_q$ signals stimulated Akt in COS-7 cells [19], whereas another paper demonstrated that an active form of $G\alpha_q$ inhibited Akt stimulation by various molecules, including $G_{\beta\gamma}$ and insulin-like growth factor, in COS-7 and HEK293 cells [20]. In addition, while we have shown that G_{11}-induced apoptosis is not mediated by phospholipase C pathways, G_q was shown to induce apoptosis via a protein kinase C-dependent pathway in CHO and COS-7 cells [5]. In neonatal ventricular myocytes, angiotensin II induces apoptosis through upregulation of intracellular Ca^{2+} [11]. We can therefore assume the existence of different $G_{q/11}$ signal systems in different cells, though the basis of discrepancies between the previous results with respect to COS-7 cells is unclear.

In the present study, we have shown that the dominant-negative mutant of RhoA inhibited carbachol-induced ROCK-I cleavage (Fig. 8), but C3 exoenzyme, RhoA subfamily specific inhibitor, was unable to inhibit it (data not shown). These results suggest that $G_{q/11}$-induced apoptosis may be regulated by not only RhoA but also other members of RhoA subfamily, RhoB and RhoC. Previous reports suggested that RhoB, but not RhoA, plays an important role in the process of cell survival [42–46] and Akt trafficking [46]. In our preliminary experiments, a constitutively active mutant of RhoB inhibited carbachol-induced ROCK-I cleavage in HeLa cells (data not shown). It may be possible that $G\alpha_{q/11}$ spatiotemporally regulates the activities of different members of the RhoA subfamily in the apoptotic process of HeLa cells, and therefore the response caused by the blockage of all members with C3 exoenzyme is different from that induced by the dominant-negative form of RhoA.

In conclusion, $G\alpha_{q/11}$ induces apoptosis by activating both protein tyrosine phosphatase and Rho in HeLa cells. Carbachol-induced apoptosis can be partially decreased by blocking the pathways singly or completely by blocking both. Our results suggest the two pathways are independently and simultaneously stimulated by Gq/11 in HeLa cells.

Acknowledgments

We thank Drs. H. Itoh and E. M. Ross for supplying the plasmids. This work was partly supported by Grants-in-Aid for Scientific Research (C) from the Japan Society for the Promotion of Science, a Grant-in-Aid for Scientific Research on Priority Areas from the Ministry of Education, Culture, Sports, Science and Technology, and grants from the Yamanouchi Research Foundation and the Naito Foundation.

References

[1] J.A. Iñiguez-Lluhi, C. Kleuss, A.G. Gilman, The importance of G-protein βγ subunits, Trends Cell Biol. 17 (1993) 230–236.
[2] D.E. Clapham, E.J. Neer, G protein βγ subunits, Annu. Rev. Pharmacol. Toxicol. 37 (1997) 167–203.
[3] J.W. Adams, Y. Sakata, M.G. Davis, V.P. Sah, Y. Wang, S.B. Liggett, K.R. Chien, J.H. Brown, G.W. Dorn II, Enhanced Gαq signaling: a common pathway mediates cardiac hypertrophy and apoptotic heart failure, Proc. Natl. Acad. Sci. U. S. A. 95 (1998) 10140–10145.
[4] J.W. Adams, A.L. Pagel, C.K. Means, D. Oksenberg, R.C. Armstrong, J.H. Brown, Cardiomyocyte apoptosis induced by Gαq signaling is mediated by permeability transition pore formation and activation of the mitochondrial death pathway, Circ. Res. 87 (2000) 1180–1187.
[5] H. Althoefer, P. Eversole-Cire, M.I. Simon, Constitutively active $G\alpha_q$ and $G\alpha_{13}$ trigger apoptosis through different pathways, J. Biol. Chem. 272 (1997) 24380–24386.
[6] S.A. Akhter, C.A. Milano, K.F. Shotwell, M.C. Cho, H.A. Rockman, R.J. Lefkowitz, W.J. Koch, Transgenic mice with cardiac overexpression of α_{1B}-adrenergic receptors. In vivo α_1-adrenergic receptor-mediated regulation of β-adrenergic signaling, J. Biol. Chem. 272 (1997) 21253–21259.
[7] S.A. Akhter, L.M. Luttrell, H.A. Rockman, G. Iaccarino, R.J. Lefkowitz, W.J. Koch, Targeting the receptor-G_q interface to inhibit in vivo pressure overload myocardial hypertrophy, Science 280 (1998) 574–577.
[8] H. Ueda, R. Morishita, H. Itoh, S. Narumiya, K. Mikoshiba, K. Kato, T. Asano, $G\alpha_{11}$ induces caspase-mediated proteolytic activation of Rho-associated kinase, ROCK-I, in HeLa cells, J. Biol. Chem. 276 (2001) 42527–42533.
[9] M.L. Coleman, E.A. Sahai, M. Yeo, M. Bosch, A. Dewar, M.F. Olson, Membrane blebbing during apoptosis results from caspase-mediated activation of ROCK I, Nat. Cell Biol. 3 (2001) 339–345.
[10] M. Sebbagh, C. Renvoize, J. Hamelin, N. Riche, J. Bertoglio, J. Breard, Caspase-3-mediated cleavage of ROCK I induces MLC phosphorylation and apoptotic membrane blebbing, Nat. Cell Biol. 3 (2001) 346–352.
[11] E. Cigola, J. Kajstura, B. Li, L.G. Meggs, P. Anversa, Angiotensin II activates programmed myocyte cell death in vitro, Exp. Cell Res. 231 (1997) 363–371.
[12] A. Bellacosa, J.R. Testa, S.P. Staal, P.N. Tsichlis, A retroviral oncogene, akt, encoding a serine–threonine kinase containing an SH2-like region, Science 254 (1991) 274–277.
[13] P.J. Coffer, J.R. Woodgett, Molecular cloning and characterisation of a novel putative protein-serine kinase related to the cAMP-dependent and protein kinase C families, Eur. J. Biochem. 201 (1991) 475–481.
[14] P.F. Jones, T. Jakubowicz, F.J. Pitossi, F. Maurer, B.A. Hemmings, Molecular cloning and identification of a serine/threonine protein kinase of the second-messenger subfamily, Proc. Natl. Acad. Sci. U. S. A. 88 (1991) 4171–4175.
[15] B.M. Burgering, P.J. Coffer, Protein kinase B (c-Akt) in phosphatidylinositol-3-OH kinase signal transduction, Nature 376 (1995) 599–602.
[16] T.F. Franke, D.R. Kaplan, L.C. Cantley, A. Toker, Direct regulation of the Akt proto-oncogene product by phosphatidylinositol-3,4-bisphosphate, Science 275 (1997) 665–668.
[17] S.K. Moule, G.I. Welsh, N.J. Edgell, E.J. Foulstone, C.G. Proud, R.M. Denton, Regulation of protein kinase B and glycogen synthase kinase-3 by insulin and β-adrenergic agonists in rat epididymal fat cells. Activation of protein kinase B by wortmannin-sensitive and-insensitive mechanisms, J. Biol. Chem. 272 (1997) 7713–7719.
[18] B. Tilton, M. Andjelkovic, S.A. Didichenko, B.A. Hemmings, M.

enjamin, G-Protein-coupled receptors and Fcγ-receptors mediate activation of Akt/protein kinase B in human phagocytes, J. Biol. Chem. 272 (1997) 28096–28101.
[19] C. Murga, L. Laguinge, R. Wetzker, A. Cuadrado, J.S. Gutkind, Activation of Akt/protein kinase B by G protein-coupled receptors. A role for α and βγ subunits of heterotrimeric G proteins acting through phosphatidylinositol-3-OH kinaseγ, J. Biol. Chem. 273 (1998) 19080–19085.
[20] R.K. Bommakanti, S. Vinayak, W.F. Simonds, Dual regulation of Akt/protein kinase B by heterotrimeric G protein subunits, J. Biol. Chem. 275 (2000) 38870–38876.
[21] C. Fan, Q. Li, D. Ross, J.F. Engelhardt, Tyrosine phosphorylation of IκB α activates NFκB through a redox-regulated and c-Src-dependent mechanism following hypoxia/reoxygenation, J. Biol. Chem. 278 (2003) 2072–2080.
[22] U.K. Laemmli, Cleavage of structural proteins during the assembly of the head of bacteriophage T4, Nature 227 (1970) 680–685.
[23] C.E. Wrede, L.M. Dickson, M.K. Lingohr, I. Briaud, C.J. Rhodes, Protein kinase B/Akt prevents fatty acid-induced apoptosis in pancreatic β-cells (INS-1), J. Biol. Chem. 277 (2002) 49676–49684.
[24] K. Kimura, T. Tsuji, Y. Takada, T. Miki, S. Narumiya, Accumulation of GTP-bound RhoA during cytokinesis and a critical role of ECT2 in this accumulation, J. Biol. Chem. 275 (2000) 17233–17236.
[25] M.O. Hengartner, The biochemistry of apoptosis, Nature 407 (2000) 770–776.
[26] K.L. Jin, S.H. Graham, X.O. Mao, X. He, T. Nagayama, R.P. Simon, D.A. Greenberg, Bax κ, a novel Bax splice variant from ischemic rat brain lacking an ART domain, promotes neuronal cell death, J. Neurochem. 77 (2001) 1508–1519.
[27] D. Stokoe, L.R. Stephens, T. Copeland, P.R. Gaffney, C.B. Reese, G.F. Painter, A.B. Holmes, F. McCormick, P.T. Hawkins, Dual role of phosphatidylinositol-3,4,5-trisphosphate in the activation of protein kinase B, Science 277 (1997) 567–570.
[28] B. Vanhaesebroeck, D.R. Alessi, The PI3K-PDK1 connection: more than just a road to PKB, Biochem. J. 346 (2000) 561–576.
[29] M.A. Lawlor, D.R. Alessi, PKB/Akt: a key mediator of cell proliferation, survival and insulin responses? J. Cell Sci. 114 (2001) 2903–2910.
[30] R. Morishita, H. Nakayama, T. Isobe, T. Matsuda, Y. Hashimoto, T. Okano, Y. Fukada, K. Mizuno, S. Ohno, O. Kozawa, K. Kato, T. Asano, Primary structure of a γ subunit of G protein, γ_{12}, and its phosphorylation by protein kinase C, J. Biol. Chem. 270 (1995) 29469–29475.
[31] A.R. Saltiel, C.R. Kahn, Insulin signalling and the regulation of glucose and lipid metabolism, Nature 414 (2001) 799–806.
[32] W. Tsai, A.D. Morielli, T.G. Cachero, E.G. Peralta, Receptor protein tyrosine phosphatase α participates in the m1 muscarinic acetylcholine receptor-dependent regulation of Kv1.2 channel activity, EMBO J. 18 (1999) 109–118.
[33] M.A. Booden, D.P. Siderovski, C.J. Der, Leukemia-associated Rho guanine nucleotide exchange factor promotes $G\alpha_q$-coupled activation of RhoA, Mol. Cell. Biol. 22 (2002) 4053–4061.
[34] H. Chikumi, J. Vazquez-Prado, J.M. Servitja, H. Miyazaki, J.S. Gutkind, Potent activation of RhoA by $G\alpha_q$ and G_q-coupled receptors, J. Biol. Chem. 277 (2002) 27130–27134.
[35] S.P. Heximer, N. Watson, M.E. Linder, K.J. Blumer, J.R. Hepler, RGS2/G0S8 is a selective inhibitor of $G_q\alpha$ function, Proc. Natl. Acad. Sci. U.S.A. 94 (1997) 14389–14393.
[36] K. Lin, D. Wang, W. Sadée, Serum response factor activation by muscarinic receptors via RhoA. Novel pathway specific to M1 subtype involving calmodulin, calcineurin, and Pyk2, J. Biol. Chem. 277 (2002) 40789–40798.
[37] H. Ueda, H. Itoh, J. Yamauchi, R. Morishita, Y. Kaziro, K. Kato, T. Asano, G protein βγ subunits induce stress fiber formation and focal adhesion assembly in a Rho-dependent manner in HeLa cells, J. Biol. Chem. 275 (2000) 2098–2102.
[38] H. Ueda, R. Morishita, J. Yamauchi, H. Itoh, K. Kato, T. Asano, Regulation of Rac and Cdc42 pathways by G_i during lysophosphatidic acid-induced cell spreading, J. Biol. Chem. 276 (2001) 6846–6852.
[39] Y. Yamaguchi, H. Katoh, K. Mori, M. Negishi, $G\alpha_{12}$ and $G\alpha_{13}$ interact with Ser/Thr protein phosphatase type 5 and stimulate its phosphatase activity, Curr. Biol. 12 (2002) 1353–1358.
[40] R.L. Boshans, S. Szanto, L. van Aelst, C. D'Souza-Schorey, ADP-ribosylation factor 6 regulates actin cytoskeleton remodeling in coordination with Rac1 and RhoA, Mol. Cell. Biol. 20 (2000) 3685–3694.
[41] A. Bose, A.D. Cherniack, S.E. Langille, S.M. Nicoloro, J.M. Buxton, J.G. Park, A. Chawla, M.P. Czech, $G\alpha_{11}$ signaling through ARF6 regulates F-actin mobilization and GLUT4 glucose transporter translocation to the plasma membrane, Mol. Cell. Biol. 21 (2001) 5262–5275.
[42] W. Du, P.F. Lebowitz, G.C. Prendergast, Cell growth inhibition by farnesyltransferase inhibitors is mediated by gain of geranylgeranylated RhoB, Mol. Cell. Biol. 19 (1999) 1831–1840.
[43] W. Du, G.C. Prendergast, Geranylgeranylated RhoB mediates suppression of human tumor cell growth by farnesyltransferase inhibitors, Cancer Res. 59 (1999) 5492–5496.
[44] A. Liu, W. Du, J.P. Liu, T.M. Jessell, G.C. Prendergast, RhoB alteration is necessary for apoptotic and antineoplastic responses to farnesyltransferase inhibitors, Mol. Cell. Biol. 20 (2000) 6105–6113.
[45] A. Liu, G.C. Prendergast, Geranylgeranylated RhoB is sufficient to mediate tissue-specific suppression of Akt kinase activity by farnesyltransferase inhibitors, FEBS Lett. 481 (2000) 205–208.
[46] I. Adini, I. Rabinovitz, J.F. Sun, G.C. Prendergast, L.E. Benjamin, RhoB controls Akt trafficking and stage-specific survival of endothelial cells during vascular development, Genes Dev. 17 (2003) 2721–2732.

THE JOURNAL OF CELL BIOLOGY

Ect2 and MgcRacGAP regulate the activation and function of Cdc42 in mitosis

Fabian Oceguera-Yanez,[1,2] Kazuhiro Kimura,[1] Shingo Yasuda,[1,2] Chiharu Higashida,[1] Toshio Kitamura,[3] Yasushi Hiraoka,[4,5] Tokuko Haraguchi,[4,5] and Shuh Narumiya[1]

[1]Department of Pharmacology and [2]Horizontal Medical Research Organization, Kyoto University Faculty of Medicine, Kyoto 606-8501, Japan
[3]Division of Cellular Therapy, Institute of Medical Science, University of Tokyo, Tokyo 108-8639, Japan
[4]Core Research for Evolutionary Science and Technology Research Project, Kansai Advanced Research Center, Kobe 651-2492, Japan
[5]Department of Biology, Graduate School of Science, Osaka University, Osaka 560-0043, Japan

Although Rho regulates cytokinesis, little was known about the functions in mitosis of Cdc42 and Rac. We recently suggested that Cdc42 works in metaphase by regulating bi-orient attachment of spindle microtubules to kinetochores. We now confirm the role of Cdc42 by RNA interference and identify the mechanisms for activation and down-regulation of Cdc42. Using a pull-down assay, we found that the level of GTP-Cdc42 elevates in metaphase, whereas the level of GTP-Rac does not change significantly in mitosis. Overexpression of dominant-negative mutants of Ect2 and MgcRacGAP, a Rho GTPase guanine nucleotide exchange factor and GTPase activating protein, respectively, or depletion of Ect2 by RNA interference suppresses this change of GTP-Cdc42 in mitosis. Depletion of Ect2 also impairs microtubule attachment to kinetochores and causes prometaphase delay and abnormal chromosomal segregation, as does depletion of Cdc42 or expression of the Ect2 and MgcRacGAP mutants. These results suggest that Ect2 and MgcRacGAP regulate the activation and function of Cdc42 in mitosis.

Introduction

During mitosis cells segregate their duplicated DNA equally to each pole and divide into two daughter cells. The cytoskeleton exerts different mechanical forces and governs this important biological process. For example, at the onset of mitosis, the instability of microtubules (MTs) increases. In prometaphase to metaphase, MTs emanating from centrosomes bind to the kinetochores of each sister chromatid. Once stabilized, the bipolar attachment of MTs to chromosomes ensures that chromosomes congress correctly at the metaphase plate. Sister chromatids are then segregated to each pole in anaphase by the combined actions of MT shrinkage and MT-associated motor proteins (Wittmann et al., 2001). In anaphase to telophase, F-actin and myosin accumulate in the cell cortex in the middle of the dividing cell to form the contractile ring, which contracts and cleaves the cell into two (Wang, 2001). Although the overall progression through mitosis is regulated by cyclin and cyclin-dependent kinase signaling, much remains to be learned about the signaling mechanism that determines the aforementioned spatio-temporal actions of the cytoskeleton.

Rho GTPases control a variety of cellular processes such as cell adhesion, cell motility, and cell contraction through induction of specific types of actin cytoskeleton and by local regulation of MT dynamics (Etienne-Manneville and Hall, 2002). Although the role of Rho in induction and maintenance of the contractile ring during cytokinesis has been well documented (Kishi et al., 1993; Mabuchi et al., 1993), the role for other Rho GTPases in the regulation of mitotic events was, until recently, unknown. *Clostridium difficile* toxin B is known to inactivate all members of Rho GTPases by selective glucosylation of the critical threonine residue (Aktories et al., 2000). We have recently found that treatment of HeLa cells with toxin B delays the progression of mitosis in prometaphase and that expression of Cdc42 mutants but not those of Rac1 or RhoA mimics this phenotype (Yasuda et al., 2004). In these cells, spindle MTs fail to bind to chromosomes in the correct bipolar manner, and chromosomes fail to congress at the metaphase plate. These findings suggest that Cdc42 plays an important role in regulating the attachment of spindle MTs to the kinetochore.

Correspondence to Shuh Narumiya: snaru@mfour.med.kyoto-u.ac.jp
K. Kimura's present address is Dept. of Ophthalmology, Yamaguchi University School of Medicine, Yamaguchi 755-8505, Japan.

Abbreviations used in this paper: CRIB, Cdc42-Rac–interacting binding domain; DH, Dbl homology; GAP, GTPase activating protein; GEF, guanine nucleotide exchange factor; MT, microtubule; PH, pleckstrin homology; RNAi, RNA interference.

The online version of this article includes supplemental material.

The Journal of Cell Biology, Vol. 168, No. 2, January 17, 2005 221–232
http://www.jcb.org/cgi/doi/10.1083/jcb.200408085

Supplemental Material can be found at:
http://www.jcb.org/cgi/content/full/jcb.200408085/DC1

Here, we extend this study to confirm the role of Cdc42 in mitosis by RNA interference (RNAi) and to further identify the regulatory mechanisms for activation and down-regulation of this Rho GTPase during cell division. Like other small GTPases, Rho GTPases cycle between the GDP-bound inactive state and the GTP-bound active state. The exchange of bound GDP for GTP is catalyzed by guanine nucleotide exchange factors (GEFs), whereas the hydrolysis of GTP by the GTPases is accelerated by GTPase activating proteins (GAPs; Zheng, 2001; Moon and Zheng, 2003). Previous studies showed that activation of Rho in mitosis is regulated by the action of a Rho exchanger, Ect2, and by the action of a Rho GAP, MgcRacGAP.

Ect2 is a GEF for Rho GTPases, containing the hallmark Dbl homology (DH) domain and pleckstrin homology (PH) domain tandem motif (Miki et al., 1993). Prokopenko et al. (1999) showed in *Drosophila melanogaster* that Pebble, the Ect2 orthologue, interacts genetically with RhoA and is required for the formation of the contractile ring and initiation of cytokinesis. Tatsumoto et al. (1999) found in mammalian cells that the inhibition of Ect2 function, either by overexpression of deletion mutants lacking the DH and PH domains or by injection of anti-Ect2 antibodies, generated multinucleated cells, indicating that Ect2 is involved in cytokinesis. They further reported that Ect2, which is localized exclusively in the nucleus of interphase cells, is released into the cytoplasm upon nuclear membrane breakdown, is localized on the spindles in metaphase, and accumulates in the cleavage furrow in telophase and then in the midbody at the end of cytokinesis. Using the pull-down assay, we previously verified the importance of Ect2 in mitotic activation of RhoA in HeLa cells (Kimura et al., 2000). We showed that GTP-RhoA accumulates in telophase, and that this accumulation can be abolished by expression of dominant-negative forms of Ect2 in synchronized HeLa cells. Although these studies have established a role for Ect2 in Rho activation and cytokinesis, little is known about its action on other Rho GTPases in mitosis. Ect2 catalyzes in vitro GDP-GTP exchange for Rac1 and Cdc42 as potently as for Rho (Tatsumoto et al., 1999).

MgcRacGAP is a Rho GAP conserved from *Caenorhabditis elegans* and *Drosophila* to mammals (Agnel et al., 1992; Toure et al., 1998; Jantsch-Plunger et al., 2000; Kawashima et al., 2000). Hirose et al. (2001) expressed a catalytically inactive mutant of MgcRacGAP, MgcRacGAP^{R386A}, and found production of multinucleate cells by this expression and suggested that this GAP is required for cytokinesis. MgcRacGAP exhibits a similar spatio-temporal localization to that of Ect2: it is present in the nucleus of interphase cells, localizes to the spindle in metaphase and anaphase, and accumulates in the midbody at the end of cytokinesis (Hirose et al., 2001). Jantsch-Plunger et al. (2000) found that a mutation in *cyk-4*, a MgcRacGAP orthologue in *C. elegans*, caused disassembly of the central spindle and failure of cytokinesis. Together these results suggest that MgcRacGAP/CYK-4 acts on RhoA and regulates cytokinesis. However, CYK-4 stimulates GTP hydrolysis of not only RhoA but also Rac1 and Cdc42 in vitro. Furthermore, in vitro MgcRacGAP exhibits greater activity toward Rac1 and Cdc42 than toward RhoA (Kawashima et al., 2000). These results raise the possibility that this molecule may also function to regulate Cdc42 and Rac1 in mitosis.

In the present work, we have adopted a variety of strategies to address the aforementioned questions. We have first synchronized HeLa cells and performed pull-down assays for the GTP-bound form of Cdc42 and Rac-1 to identify mitosis-associated changes in the activation of these two GTPases. We have examined the effects of the expression of the dominant-negative forms of Ect2 and MgcRacGAP, or RNAi of Ect2, on the level of GTP-bound Cdc42 and Rac1 during mitosis. We have also investigated mitotic phenotypes of cells either subjected to RNAi for Cdc42 and Ect2, or overexpressing the aforementioned Ect2 and MgcRacGAP mutants. Our results indicate that Ect2 and MgcRacGAP regulate the activation and function of Cdc42 in mitosis.

Results

Changes in the levels of GTP-bound Cdc42 and Rac during mitosis

We used thymidine and nocodazole either alone or in combination to enrich HeLa S3 cells in G2 phase, prometaphase, metaphase, telophase, and G1 phase, as described in Materials and methods. To clarify the activation of Cdc42 and Rac in cell division, we used a GST fusion of the Cdc42-Rac–interacting binding domain (CRIB) of Pak1 (GST-CRIB-Pak; Matsuo et al., 2002) to pull-down the GTP-bound forms of Rac1 or Cdc42 from the lysates of these cells. We then subjected fractions of the precipitates to immunoblot analysis for Cdc42 and Rac, using antibodies specific to each GTPase. The amounts of the GTP-bound form of each GTPase were then quantified. GTP-bound Cdc42 accumulated to some extent during G2 phase. After nocodazole removal, the level of GTP-Cdc42 decreased in prometaphase, elevated transiently in metaphase, reaching a level similar to that found for G2/G1 phases, and then decreased again in telophase (Fig. 1 A). However, the level of GTP-bound Rac1 did not change significantly during mitosis (Fig. 1 A). As a reference, we also monitored the change in GTP-Rho, which, in agreement with previous findings (Kimura et al., 2000), peaked in telophase (Fig. 1 A).

Ect2 and MgcRacGAP regulate activation of Cdc42 during mitosis

The NH_2-terminal fragment of Ect2 lacking the DH-PH domain (Ect2-N1) functions as a dominant-negative mutant and suppresses Rho activation in telophase (Tatsumoto et al., 1999; Kimura et al., 2000). To test if Ect2 is involved in the activation of Cdc42 in metaphase, we overexpressed this Ect2 mutant in mitotic HeLa cells and performed pull-down assays with lysates from these cells. Expression of Ect2-N1 suppressed the accumulation of GTP-bound Cdc42 in metaphase to the level found in prometaphase. As a consequence, the level of GTP-Cdc42 remained low from prometaphase to telophase in the Ect2-N1–overexpressing cells (Fig. 1 B). However, Ect2-N1 expression had no effect on the level of GTP-bound Rac1 (Fig. 1, A and B).

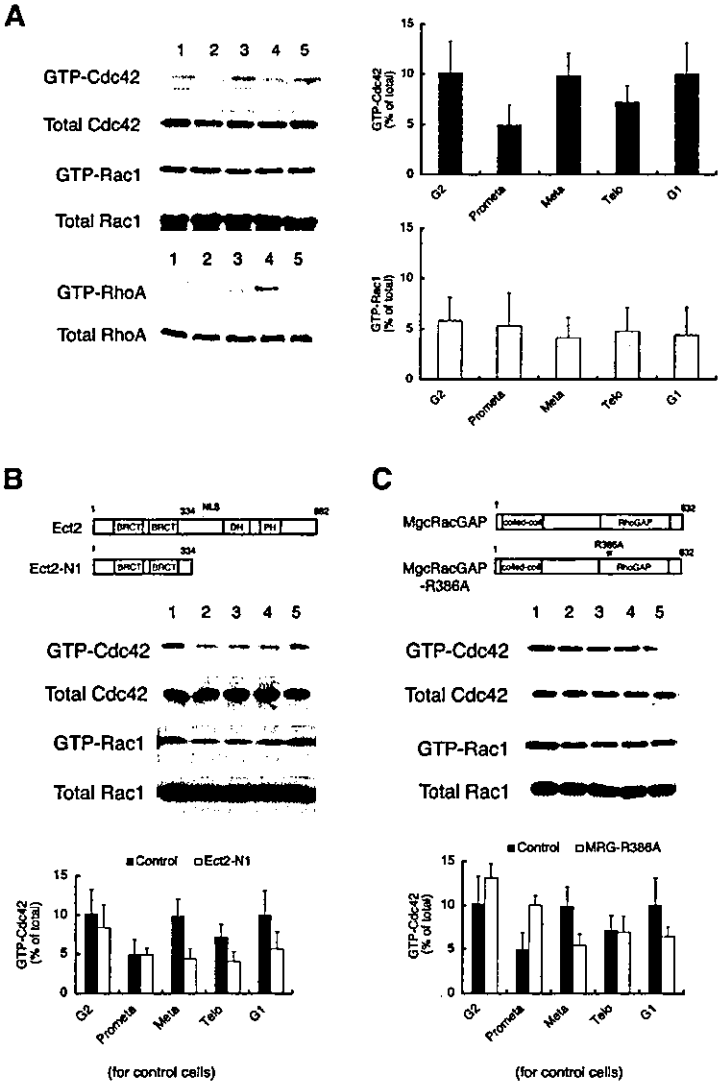

Figure 1. **Regulation of Cdc42 activation in mitosis by Ect2 and MgcRacGAP.** (A) Cell cycle–associated changes in the level of the GTP-bound form of each Rho GTPase. HeLa S3 cells were synchronized, collected in G2 phase (lane 1), prometaphase (lane 2), metaphase (lane 3), telophase (lane 4), and G1 phase (lane 5), respectively, and subjected to the pull-down assay to detect GTP-Cdc42 or GTP-Rac, as described in Materials and methods. Typical immunoblots are shown on the left, and the results of the quantitative analysis are on the right. Values are shown as means ± SEM ($n = 4$ and 3 for Cdc42 and Rac, respectively). (B) Suppression of Cdc42 activation in metaphase by expression of a dominant-negative mutant of Ect2. Synchronized HeLa cells were transfected with pCEV32F-Ect2-N1, collected at various phases of the cell cycle, and subjected to the pull-down assay as described in Materials and methods. The top diagram shows the domain structures of full-length Ect2 and Ect2-N1 (BRCT, BRCA carboxyl terminus domain; DH, Dbl homology domain; PH, pleckstrin homology domain; NLS, nuclear localization signal). The middle panel is representative of a typical experiment, and the bottom panel represents the results of quantitative analysis of three independent experiments (open bars, experiments with Ect2-N1; closed bars, the control experiment shown in A). (C) Prevention of down-regulation of Cdc42 by expression of a catalytically inactive mutant of MgcRacGAP. Synchronized HeLa cells were transfected with pME18S-MgcRacGAP^{R386A}, collected at various phases of the cell cycle, and subjected to the pull-down assay as described in Materials and methods. Top diagrams show the structure of MgcRacGAP and MgcRacGAP^{R386A} (coiled-coil, coiled-coil domain; RhoGAP, GTPase activating homology domain). The middle panel is representative of a typical experiment, and the bottom panel represents the results of quantitative analysis of three independent experiments (open bars, experiments with MgcRacGAP^{R386A}; closed bars, the control experiment shown in A).

Next, we investigated the involvement of MgcRacGAP in the regulation of Cdc42 activation in mitosis. To this end, we used MgcRacGAP^{R386A}, a mutant that is devoid of GAP activity and that is known to produce multinucleate cells when overexpressed (Hirose et al., 2001). We transfected thymidine-synchronized HeLa cells with this GAP mutant and overexpressed the mutant protein in mitotic cells. The lysates of the transfected cells were then subjected to the pull-down assay. Overexpression of MgcRacGAP^{R386A} elevated the amount of GTP-Cdc42 in prometaphase to a level comparable to that found in metaphase in control cells (Fig. 1 C), resulting in premature accumulation of GTP-Cdc42. Curiously, MgcRacGAP^{R386A} expression tended to suppress the Cdc42 activation thereafter (see Discussion). In contrast, the MgcRacGAP^{R386A} expression had little effect on the activation of Rac1 (Fig. 1 C).

We confirmed the aforementioned findings by depletion of endogenous Ect2 with RNAi. As shown in Fig. 2 A, the treatment of HeLa cells with RNAi for Ect2 potently suppressed the expression of the endogenous protein to <20% of that found in control cells after 48 h. We then examined the accumulation of GTP-Cdc42 in cells subjected to RNAi. Although cells subjected to control RNAi exhibited an accumulation of GTP-Cdc42 in metaphase, no accumulation was found in cells subjected to Ect2 RNAi (Fig. 2 B). We also wished to verify the role of MgcRacGAP by RNAi, but we were unable to obtain a significant decrease of this protein by the RNAi strategy we used for Ect2. These results suggest that Ect2 and MgcRacGAP regulate the level of GTP-Cdc42 in mitosis, the former activating Cdc42 in metaphase and the latter suppressing Cdc42 activation in prometaphase. Interestingly,

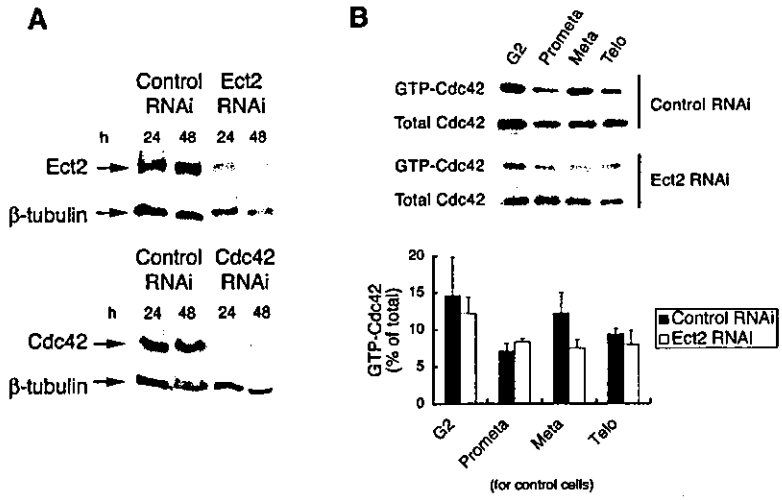

Figure 2. **RNAi for Ect2 and its effects on accumulation of GTP-Cdc42 in metaphase.** (A) Depletion of Cdc42 or Ect2 by RNAi. HeLa cells were subjected to RNAi for Ect2 (Ect2 RNAi), Cdc42 (Cdc42 RNAi), or *E. coli* LacZ (control RNAi). After 24 and 48 h, the cells were lysed and subjected to immunoblot with the respective antibody. (B) Effects of Ect2 depletion on accumulation of GTP-Cdc42 in metaphase. HeLa S3 cells were transfected with control or Ect2 siRNA after the first thymidine block. The cells then underwent a second thymidine block and, after release from this block, were collected at different phases of the cell cycle and subjected to the pull-down assay. One sixth of the precipitates and one twentieth of the supernatant were used to show the amount of GTP-Cdc42 and total Cdc42, respectively. The top panel represents typical immunoblots and the bottom represents the results of quantitative analysis of three independent experiments (closed bars, experiments with control RNAi; open bars, Ect2 RNAi experiment). Values are shown as means ± SEM ($n = 3$).

neither Ect2 nor MgcRacGAP appears to regulate Rac activation in mitosis, although they show catalytic activity toward Rac in vitro.

RNAi for Cdc42 or Ect2 causes a delay in metaphase progression

We have recently suggested that Cdc42 regulates the bi-oriented attachment of spindle MTs to kinetochores during metaphase (Yasuda et al., 2004). This suggestion was based on experimental findings using toxin B and Cdc42 mutants. Here, we confirmed these findings by depletion of Cdc42 with RNAi, and also by depletion of Ect2. As with RNAi for Ect2, RNAi for Cdc42 in HeLa cells effectively suppressed expression of the endogenous protein to <10% of that found in control cells (Fig. 2 A). Therefore, we transfected HeLa cells with the respective RNAi and cultured the cells for 50 h, during which time they were subjected to a double thymidine block to synchronize the cell cycle progression. Cells were collected at different time points after release from the second thymidine block and then subjected to flow-cytometry analysis. We found that whereas cells subjected to control RNAi or RNAi for Cdc42 or Ect2 progressed through S phase at comparable rates, exit from mitosis was consistently delayed in the cells subjected to Cdc42 or Ect2 RNAi when compared with control RNAi cells; percentages of cells with 4N DNA content 11 h after thymidine release were 33, 32, and 33 for control, Cdc42, or Ect2 RNAi cells, respectively; by 12 h, percentages were 26, 32, and 33; and by 15 h, they were 18, 24, and 26. The cells were then fixed 12 h after release, and the mitotic index of each population was determined by staining for MTs and chromosomes (Fig. 3 A). The mitotic index of control RNAi cells was <9%, whereas the indexes for Cdc42 and Ect2 RNAi cells were significantly higher and were 22 and 19%, respectively. Interestingly, combined RNAi for Cdc42 and Ect2 together increased the mitotic index (17.5%) to nearly the values observed with RNAi for either alone. This lack of synergy is consistent with our hypothesis that Ect2 and Cdc42 work in the same pathway. Immunofluorescence analysis of mitotic cells in these populations revealed that although the majority of cells had formed a bipolar spindle, chromosomal congression was often impaired; in some cells, chromosomes were widely scattered and in others some chromosomes remained around either pole (Fig. 3 B). Quantitative analysis revealed that the proportion of cells that showed such misaligned chromosomes was significantly higher in the Cdc42- or Ect2-depleted cell population when compared with the control cell population (Fig. 3 C). Consequently, the proportion of cells in metaphase was significantly lower in the Cdc42- or Ect2-depleted cell populations. Staining of these cells both for CENP-A, a kinetochore protein, and Mad2 revealed the presence of Mad2 at a significant number of kinetochores (Fig. 3 D). Mad2 associates with the kinetochore in the absence of spindle MT binding where it functions to arrest cell cycle progression, thus ensuring that the cell progresses to anaphase only when all kinetochores have attached with spindle MTs (Cleveland et al., 2003). These results indicate the loss of MT attachment to kinetochores in cells where either Cdc42 or Ect2 or both of these proteins have been depleted. Interestingly, however, significant proportions of the cells subjected to RNAi for Ect2 or Cdc42 nonetheless progressed to anaphase and subsequently to telophase. Consistently, most of these cells progressed to G1, resulting in cells with micro- and macronuclei (Fig. 3, C and E). These results suggest that the spindle checkpoint mechanism was impaired in these cell populations. Our previous work showed that Cdc42 acts on its effector, mDia3, which localizes to kinetochores in mitosis, and that toxin B treatment disrupts this localization (Yasuda et al., 2004). We wondered if depletion of Ect2 or Cdc42 has similar effects on mDia3 localization. We found that, although the mDia3 signals were seen as small punctate spots next to those of CENP-A in control RNAi cells, these signals became diffuse and blurred upon Ect2/Cdc42 depletion (Fig. 3 F).

To gain a greater insight into this process, we used video microscopy to monitor the mitotic progression of cells subjected to Ect2 or Cdc42 depletion. Whereas the control cells

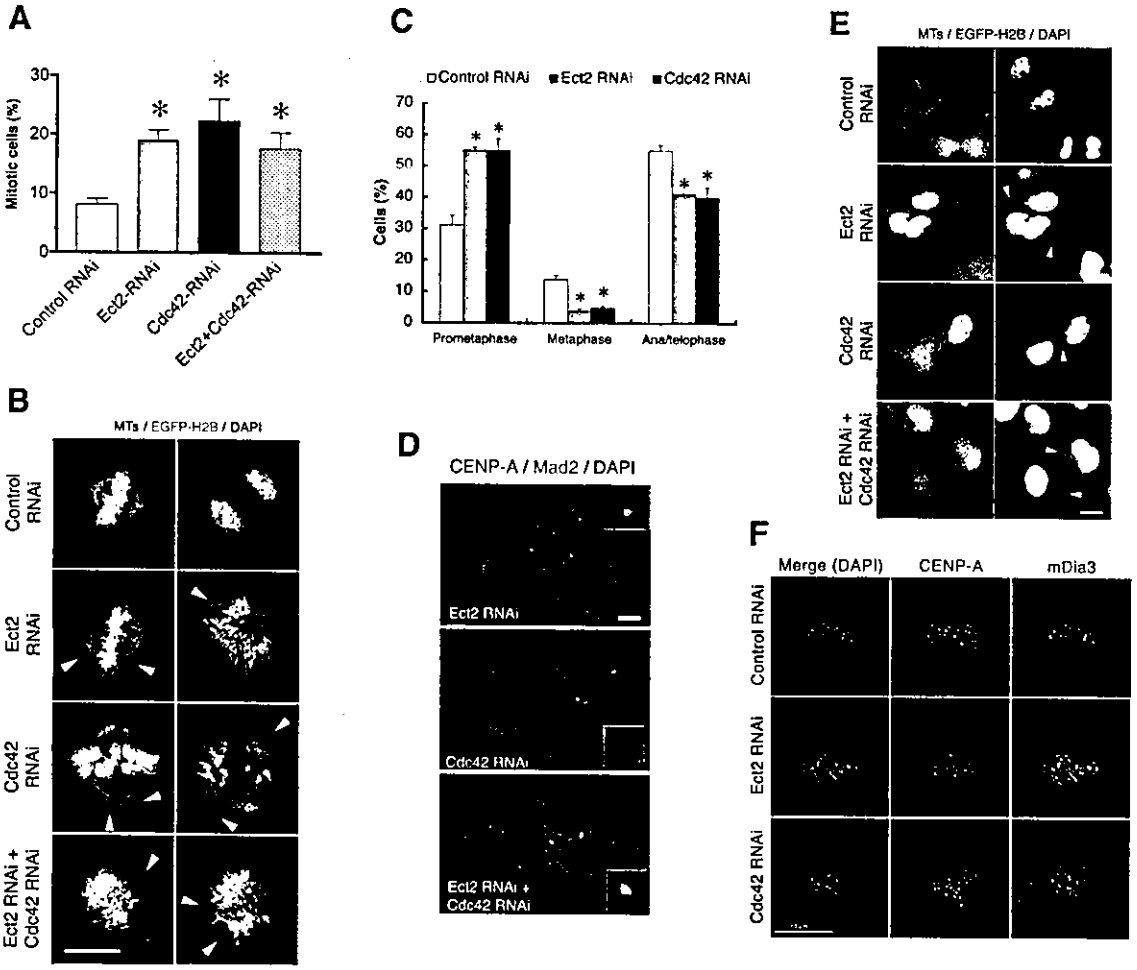

Figure 3. **Prometaphase delay by RNAi for Cdc42 or Ect2 in HeLa cells.** (A) Mitotic index. Cells subjected to RNAi were synchronized in S phase by double thymidine block, and were fixed at 12 h after release from the second block. The RNAi cells were identified by coexpression of pEGFP-histone H2Bk. The cells were stained for MTs and chromosomes and the mitotic index was calculated by examining more than 250 cells in each of four independent experiments. Results are the mean ± SEM ($n = 4$). *, $P < 0.05$ versus control RNAi cells. (B) Immunofluorescence. Cells treated as in A and expressing EGFP-H2Bk (green) were stained for chromosomes (DAPI, blue) and β-tubulin (red). Arrowheads indicate misaligned chromosomes. (C) Prometaphase delay. Mitotic cells in each population were examined and the percentages of cells in prometaphase (cells with misaligned chromosomes), metaphase (cells with chromosomes aligned at the metaphase plate), or ana/telophase (cells showing chromosome segregation) were determined. Results are mean ± SEM ($n = 3$). (D) Mad2 staining. Cells treated as in A were subjected to staining for Mad2 (green), CENP-A (red), and chromosomes (DAPI, blue). Insets are enlargements of the indicated regions of interest. (E) Production of aberrant multinucleate cells. Cells subjected to respective RNAi were fixed at 14 h after the release and stained for β-tubulin (red) and chromosomes (DAPI, blue and right column). Arrowheads show micronuclei. (F) mDia3 localization. HeLa cells subjected to control RNAi or RNAi for Ect2 or Cdc42 were subjected to staining for mDia3 (green), CENP-A (red), and with DAPI (blue). Bars: (B, E, and F) 10 μm; (D) 2 μm.

progressed from prometaphase to telophase within 50 min (Fig. 4 A and Video 1, available at http://www.jcb.org/cgi/content/full/jcb.200408085/DC1), chromosomes in cells subjected to Ect2 RNAi took longer to assemble at the metaphase plate, and this assembly was never quite complete. In many cells, some chromosomes remained adjacent to either pole, whereas the majority appeared to assemble at the metaphase plate (Fig. 4 B and Video 2, available at http://www.jcb.org/cgi/content/full/jcb.200408085/DC1). A similar phenotype was observed in cells subjected to RNAi for Cdc42 alone (Fig. 4 C and Video 3, available at http://www.jcb.org/cgi/content/full/jcb.200408085/DC1) or both Ect2 and Cdc42 together (not depicted). In addition, depletion of Ect2 resulted in failure of cytokinesis in 40% of the cells observed ($n = 19$), thus confirming the role of Ect2 in the regulation of cytokinesis. Together, these results confirm our previous suggestion that Cdc42 regulates the bipolar attachment of spindle MTs to kinetochores before chromosome congression in metaphase and further suggest that Ect2 regulates the activation of Cdc42 during this process.

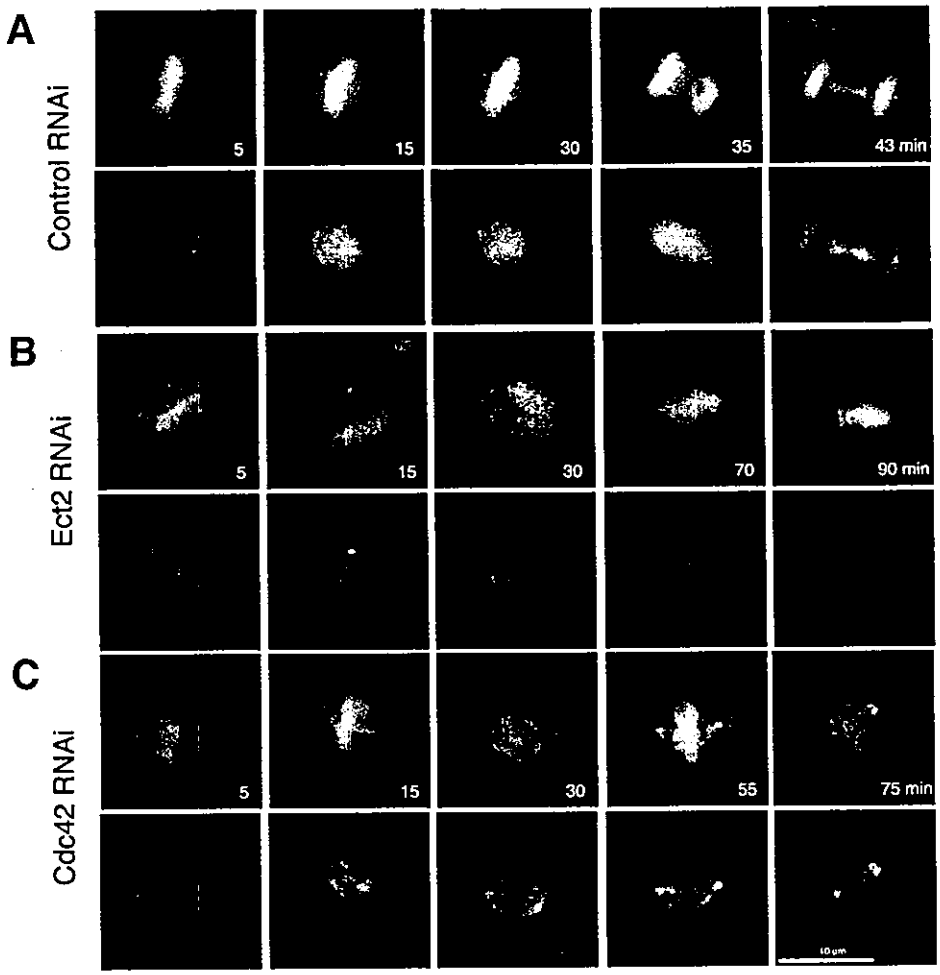

Figure 4. **Ect2 and Cdc42 depletion induce abnormalities in chromosome alignment and segregation in HeLa cells.** HeLa cells were cotransfected with pEGFP-EB1 and pDsRed2-histone H2Bk together with control siRNA (A), Ect2 siRNA (B), or Cdc42 siRNA (C) and time-lapse imaging was taken after 48 h. The bottom panels of each set show the EGFP-EB1 images only. The movies of these time-lapse acquisitions are available online as Videos 1–3 (available at http://www.jcb.org/cgi/content/full/jcb.200408085/DC1).

Expression of dominant-negative Ect2 and MgcRacGAP mutants causes prometaphase delay

The aforementioned role of Ect2 was further confirmed by expression of the dominant-negative mutant Ect2-N1. HeLa cells were synchronized with thymidine in early S phase and transfected with Ect2-N1. The cells were released from the thymidine block and enriched in mitosis by the use of nocodazole. The cells were then allowed to enter and progress through mitosis upon nocodazole removal. At 120 min after nocodazole removal, the majority of control cells expressing GFP had reached the end stage of telophase (Fig. 5 A, a and b). When we expressed Ect2-N1 in mitotic cells, we observed a significant increase in the number of binucleate cells containing two nuclei of equal size (Fig. 5 A, c and d) as reported previously (Tatsumoto et al., 1999; Kimura et al., 2000). However, the more striking observation is the accumulation of cells showing aberrant nuclei with nuclear invaginations and micronuclei (Fig. 5 A, e and f), and also of cells arrested in prometaphase with scattered chromosomes (Fig. 5 A, g and h). Immunostaining revealed that Mad2 was present at some kinetochores of condensed chromosomes in prometaphase-arrested cells, suggesting the absence of MT attachment to these kinetochores (Fig. 5 B). Quantification of the numbers of the cells showing these phenotypes revealed statistically significant increases in the number of cells showing each phenotype upon Ect2-N1 expression compared with GFP expression (10.2 vs. 4.4% for binucleated cells, 13.2 vs. 3.3% for cells with abnormal nuclei, and 20 vs. 9.6% for cells in prometaphase; Fig. 5 C). Accumulation in prometaphase and aberrant nuclear shape were also noted in cells expressing CRIB-Pak, a protein motif capable of trapping the active form of Cdc42 (Fig. S1, available at http://www.jcb.org/cgi/content/full/jcb.200408085/DC1).

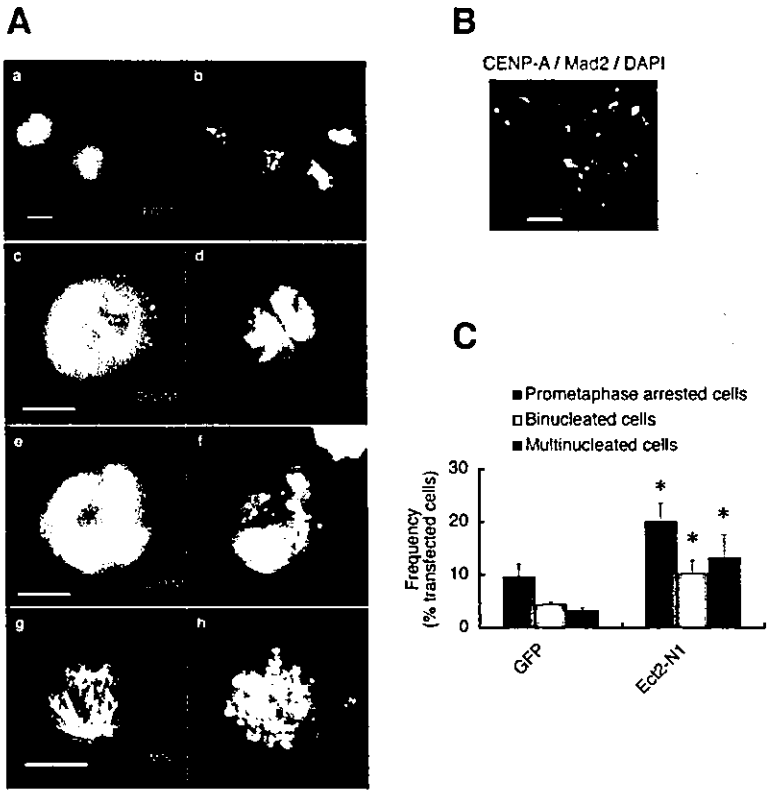

Figure 5. **Effects of overexpression of Ect2-N1 on mitosis of HeLa cells.** (A) Mitotic phenotype. HeLa cells synchronized in S phase were transfected with pEGFP (a and b) or pEGFP-Ect2-N1 (c–h). The cells were fixed 120 min after nocodazole removal and subjected to fluorescence microscopy for GFP (a, c, and e, green), anti–β-tubulin staining (g, green), and DAPI (a–h, blue). The Ect2-N1-expressing cells show the binucleate phenotype (c and d), the multinucleate phenotype with macro- and micronuclei (e and f), or the prometaphase arrest (g and h). (B) Mad2 staining. The Ect2-N1–expressing cells were treated as in A and stained for CENP-A (red), Mad2 (green), and chromosomes (DAPI, blue). Positive Mad2 staining was detected at some kinetochores. (C) Quantitative analysis of the mitotic phenotypes of the cells expressing Ect2-N1. These experiments were repeated seven times, and the numbers of cells showing each mitotic phenotype were determined in more than 200 cells each experiment. Results shown are the mean ± SEM ($n = 7$). *, $P < 0.05$ versus each corresponding subpopulation of the pEGFP-transfected cells. Bars: (A) 10 μm; (B) 2 μm.

Next, we expressed MgcRacGAP^{R386A} in mitotic cells and examined the effect of MgcRacGAP inactivation on mitosis essentially in the same manner as described for Ect2-N1. Expression of MgcRacGAP^{R386A} not only induced binucleate cells containing two nuclei of equal size (Fig. 6 A, a and b), as reported previously (Hirose et al., 2001), but also caused the accumulation of cells with aberrant nuclei with nuclear invaginations and micronuclei (Fig. 6 A, c and d) and the accumulation of cells arrested in prometaphase with scattered chromosomes (Fig. 6 A, e and f). Again, immunostaining revealed that Mad2 was present at the kinetochores of some condensed chromosomes in prometaphase-arrested cells (Fig. 6 B). Quantification revealed that 9.4, 6.3, and 21.6% of the MgcRacGAP^{R386A}-transfected cells were binucleate, multinucleate with aberrant shape, and arrested in prometaphase, respectively (Fig. 6 C). We found that expression of Cdc42^{G12V} resulted in the production of comparable populations of cells exhibiting these three mitotic phenotypes (Fig. 6 C). These results, together with those observed in the pull-down assay (Fig. 1 C), have verified the participation of MgcRacGAP in the regulation of Cdc42 in mitosis.

Cell cycle–associated changes in the spatial localization of Cdc42

The aforementioned results strongly suggest that Cdc42 works spatio-temporally in the mitosis of mammalian cells. To investigate the localization of endogenous Cdc42 during the cell cycle, we stained for Cdc42 in HeLa cells in different phases of mitosis. We tested the specificity of the antibody against Cdc42 by Western blot analysis of HeLa cell lysates. This antibody recognized a single band in HeLa cell lysates, the intensity of which could be increased in a sample enriched in Cdc42 using GST-CRIB-Pak beads (Fig. 7 A). The specificity of the antibody was further verified by Cdc42 RNAi, as the intensity of the band recognized by this antibody decreased with depletion of the endogenous protein (Fig. 2 A). This antibody was then used for immunofluorescence studies to determine the localization of endogenous Cdc42 in mitotic HeLa cells. The most prominent feature observed using this antibody was the appearance of a spindle shape signal in metaphase cells (Fig. 7 B). Costaining for β-tubulin revealed that this signal was localized along MTs of the mitotic spindle and that the signal was more concentrated at the minus-end region of these MTs. The addition of either the immunogenic peptide (Fig. 7 C) or recombinant GST-Cdc42 (not depicted) abolished this signal, suggesting that it represented endogenous Cdc42. Furthermore, staining for Rho under identical conditions did not reveal any specific signal (unpublished data). The Cdc42 signal localized in the spindle MTs of prometaphase cells, moved to the central spindle as cells progressed through anaphase to telophase, and finally concentrated in the intercellular bridge formed between two daughter cells at the end of cytokinesis (Fig. 7 B). When costaining for MgcRacGAP was conducted, the MgcRacGAP

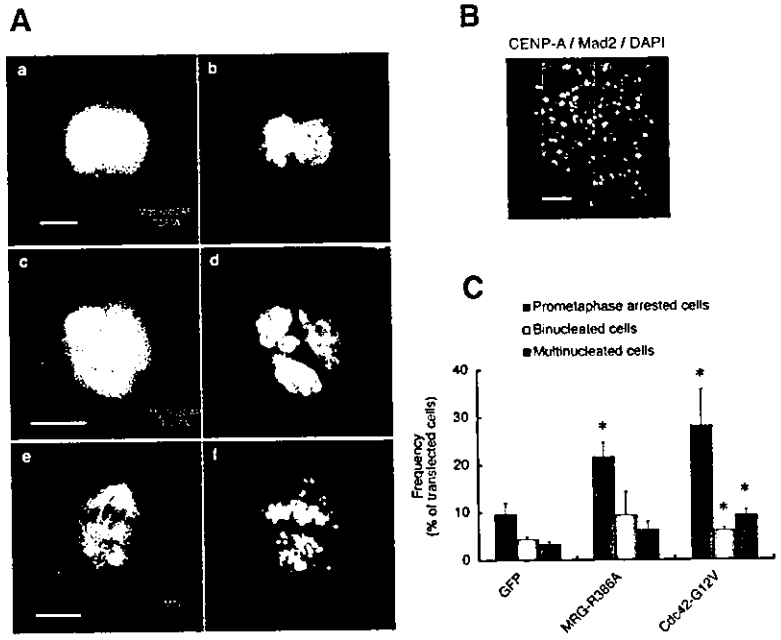

Figure 6. **Effects of overexpression of MgcRacGAP^{R386A} on mitosis of HeLa cells.** (A) Mitotic phenotypes. HeLa cells synchronized in S phase were transfected with either pEGFP alone or pEGFP and pME18S-MgcRacGAP^{R386A} (a–f). At 120 min after nocodazole removal, the cells were fixed and subjected to fluorescence microscopy for GFP (a and c, green), anti–β-tubulin staining (e, green), and DAPI (a–f, blue). MgcRacGAP^{R386A}-expressing cells show the binucleate phenotype (a and b), the multinucleated phenotype with macro- and micro-nuclei (c and d), or the prometaphase arrest (e and f). (B) Mad2 staining. The MgcRacGAP^{R386A}-expressing cells were treated as in A and stained for CENP-A (red), Mad2 (green), and chromosomes (DAPI, blue). Positive Mad2 staining was detected at some kinetochores. (C) Quantitative analysis of the mitotic phenotypes of the cells expressing MgcRacGAP^{R386A}. The mitotic phenotype of HeLa cells expressing GFP, MgcRacGAP^{R386A} (MRG-R386A), or Cdc42^{G12V} was examined in more than 200 cells for each experiment, and the percentages of cells showing prometaphase arrest, binucleate, or aberrant multinucleate phenotypes were determined. Results represent the mean ± SEM ($n = 7$). *, $P < 0.05$ versus each corresponding subpopulation of the pEGFP-transfected cells. Bars: (A) 10 μm; (B) 2 μm.

signal was also seen on spindle MTs from prometaphase to telophase and partially colocalized with the Cdc42 signal. However, the signals for the two molecules began to separate in late anaphase, and, at the end of cytokinesis, the MgcRacGAP signal no longer overlapped with that of Cdc42; the former concentrated in the Fleming body and the latter on the bridge on either side of it.

To test whether or not the distribution of the Cdc42 signal on the spindle MTs was under regulation of Ect2 and MgcRacGAP, we expressed dominant-negative mutants of these molecules in mitotic HeLa cells and performed Cdc42 immunostaining (Fig. 7 D). In the cells transfected with MgcRacGAP^{R386A}, the Cdc42 signal was observed all along the spindle MTs, reaching the vicinity of the kinetochores, where the MgcRacGAP signal was also observed (Fig. 7 D; 65% of 20 transfected cells). In contrast, when EGFP-Ect2-N1 transfection was performed, the Ect2-N1 signal was distributed from the vicinity of the kinetochores on chromosomes to the plus-end region of the mitotic spindle, and the Cdc42 signal became more limited to the minus-end region of the spindle in the vicinity of the centrosomes (61% of 23 transfected cells).

Discussion

We recently conducted a series of experiments using toxin B and various Rho GTPase mutants, and examined their role in mitosis (Yasuda et al., 2004). The results of these experiments indicate that Cdc42 acts on its downstream target, mDia3, and facilitates bi-orient attachment and stabilization of spindle MTs to kinetochores. Here, we have adopted several strategies to extend this study and, further, to clarify the pathway regulating Cdc42 in mitosis. First, we used the pull-down assay for GTP-Cdc42, and found accumulation of GTP-Cdc42 in metaphase of HeLa S3 cells, which is consistent with the proposed action of Cdc42 in metaphase. Second, we expressed dominant-negative forms of Ect2 and MgcRacGAP, a GEF and a GAP of Rho GTPases in mitosis, respectively, or depleted Ect2 by RNAi, and found that the aforementioned accumulation of Cdc42 in metaphase was abolished by these procedures. Third, we performed RNAi for Cdc42 and Ect2 or expressed the dominant-negative mutants of Ect2 and MgcRacGAP, and found that these procedures cause the prometaphase delay similar to that found in the previous study. Finally, using immunofluorescence, we found that a subpopulation of Cdc42 is associated with the spindle MTs and that its localization is regulated by the activities of Ect2 and MgcRacGAP. These results strongly argue that Ect2 and MgcRacGAP regulate the activation and function of Cdc42 in mitosis.

Regulation of Cdc42 in mitosis by Ect2 and MgcRacGAP is intriguing, given previous findings that the two molecules regulate Rho in mitosis (Tatsumoto et al., 1999; Kimura et al., 2000; Jantsch-Plunger et al., 2000; Hirose et al., 2001; Minoshima et al., 2003). These results, together with our current findings, indicate that the same GEF and GAP can regulate two different Rho GTPases, Cdc42 and Rho, in different phases of mitosis. Both Ect2 and MgcRacGAP are present in interphase nuclei, are released to the cytoplasm after nuclear envelope breakdown, associate with the spindle MTs, and change their localization during cell division (Tatsumoto et al., 1999; Hirose et al., 2001). These results indicate that they associate with different proteins in different phases of mitosis and/or are modified differently. It is tempting to think that such interactions

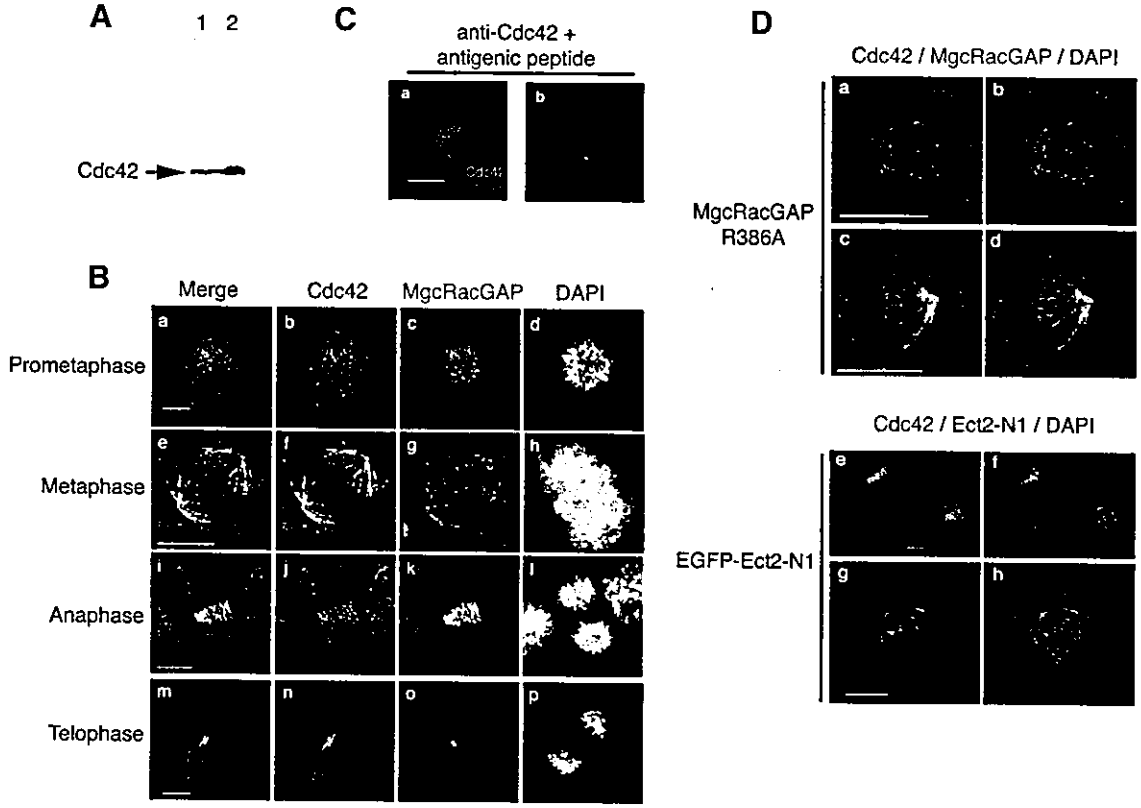

Figure 7. **Localization of Cdc42 in mitotic cells.** (A) Specificity of the antibody to Cdc42. One fiftieth of HeLa cell extracts from one 10-cm dish (lane 1) or one fourth of the pull-down precipitates of lysates from four dishes of HeLa cells at metaphase using the GST-CRIB-Pak (lane 2) were probed with the monoclonal anti-Cdc42 antibody. (B) Cdc42 localization in mitotic HeLa S3 cells. Randomly growing HeLa S3 cells were preextracted for 1 min with 0.5% Triton X-100 in PHEM, fixed, and stained for Cdc42 (green), MgcRacGAP (red), and chromosomes (DAPI, blue). Immunofluorescence images of the cells in each phase of mitosis are shown. (C) Competition experiments. The cells were treated as in B and subjected to staining for Cdc42 (red) and chromosomes (DAPI, blue) in the presence of the immunogenic peptide. A single representative cell in metaphase is shown (a, merged image; b, staining for Cdc42 alone). (D) Effects of MgcRacGAP^{R386A} or Ect2-N1 expression on distribution of Cdc42 on the metaphase spindle. The cells were cotransfected with MgcRacGAP^{R386A} together with EGFP (a–d) to allow the identification of transfected cells, or with EGFP-Ect2-N1 (e–h) and treated as in B. Chromosomes were stained with DAPI (a, c, e, and g, blue). Cdc42 was stained with monoclonal anti-Cdc42 antibody and detected with goat anti–mouse IgG coupled to Alexa-647 and pseudo-colored to green (a–d) or with donkey anti–mouse IgG coupled to Alexa-594 shown in red (e–h). MgcRacGAP is shown in red (a–d). EGFP-Ect2-N1 is shown in green (e–h). Two different optical sections of a single cell are shown each in a and b and c and d. Bars, 10 μm.

and/or modifications determine not only their localization but also their specificity. For example, the NH_2-terminal domain of Ect2 that we used in these experiments contains the tandem BRCT domains. It was reported recently that the tandem BRCT domains have affinity for phospho-proteins (Yu et al., 2003). Therefore, it is likely that the BRCT domain of Ect2 binds to specific phosphorylated proteins, which in turn provide signals that dictate the specificity of Ect2. Ect2 might bind to different phospho-proteins in metaphase and telophase, which then may provide the phase-specific specificity of this exchanger. Moreover, a subpopulation of Ect2 is phosphorylated early in mitosis (Tatsumoto et al., 1999; Kimura et al., 2000). Experimental evidence for, and an implication of such an interaction and modification, are clearer for MgcRacGAP. Recently, Ban et al. (2004) reported that MgcRacGAP binds PRC1, a mitotic CDK substrate, and that this binding inhibits MgcRacGAP activity toward Cdc42 in metaphase. This finding can explain how Cdc42 is activated in metaphase in spite of its colocalization with MgcRacGAP on the metaphase spindle (Fig. 7 B). It is also known that covalent modification of MgcRacGAP changes its substrate specificity. Minoshima et al. (2003) found that phosphorylation of MgcRacGAP by Aurora kinase B induces latent GAP activity toward RhoA, and this activity is important for down-regulation of Rho at the end of cytokinesis. Thus, it appears that both Ect2 and MgcRacGAP work on Cdc42 around metaphase, whereas they act on RhoA late in mitosis. It is intriguing that the expression of MgcRacGAP^{R386A} elevated the level of GTP-Cdc42 in prometaphase but tended to suppress the Cdc42 activation in metaphase. We do not have an experimental explanation for the latter effect. It may be a secondary effect due to the prometaphase arrest induced by this MgcRacGAP mutant. In addition, Somers and Saint (2003) found asso-

ciation of a *Drosophila* MgcRacGAP orthologue, RacGAP50C, with a *Drosophila* Ect2 orthologue, Pebble, during mitosis. Therefore, it is possible that overexpressed MgcRacGAP^{R386A} binds to endogenous Ect2 and affects its activity.

Here, we performed RNAi for Cdc42 and Ect2 and found that depletion of either protein induces prometaphase delay, which is essentially similar to that found in cells subjected to toxin B treatment, overexpression of Cdc42 mutants, and RNAi for mDia3 (Yasuda et al., 2004). Furthermore, we found that expression of MgcRacGAP^{R386A} also interfered with the transition to metaphase in a similar way. This, although apparently paradoxical, is consistent with our finding that both dominant-active and dominant-negative Cdc42 mutant induced the delay in prometaphase, and can be explained by misorientation of the spindle MTs by ectopic expression of an excess amount of active Cdc42. Although dominant-active and dominant-negative Cdc42 mutants induce the opposing actin phenotypes, they cause the same phenotype with respect to MT targeting in interphase cells (Etienne-Manneville and Hall, 2001). These results not only corroborated the role of Cdc42 in the MT attachment to kinetochores but also that Ect2 and MgcRacGAP regulate this Cdc42 function. In contrast, previous studies have shown that interfering with Ect2 and MgcRaGAP causes cytokinesis failure, which led the authors to suggest that Ect2 and MgcRacGAP are linked mainly with RhoA (Tatsumoto et al., 1999; Jantsch-Plunger et al., 2000; Kimura et al., 2000; Hirose et al., 2001). However, though not explicitly described in the previous papers, the tetraploid nucleus in these cells was abnormal in shape. Furthermore, Van de Putte et al. (2001) reported that homozygous disruption of the gene for MgcRacGAP resulted in death of E3.5–4 embryos due to the failure of chromosomal segregation. In addition, expression of active forms of Pak, an effector of Cdc42, resulted in the production of cells with multiple spindles (Vadlamudi et al., 2000), and an endogenous Pak isoform, Pak 1, was shown to localize at the kinetochore in mitotic cells (Li et al., 2002). Recently, Tatsumoto et al. (2003) used *Xenopus laevis* mitotic extracts and examined in vitro the effect on mitosis of anti-Ect2 antibody as well as dominant-negative forms of Ect2 and Rho GTPases. They found that addition of either anti-Ect2 antibody or dominant-negative Ect2 or Cdc42 interfered with normal progression of metaphase by causing many misaligned chromosomes, a phenotype very similar to that found in HeLa cells in this study. These results add further support to the role of Ect2 and Cdc42 in mitosis.

Thus, our current findings indicate that Cdc42 is essential in mitosis. Curiously, however, Chen et al. (2000) established a Cdc42 null cell line from ES cells by disruption of the Cdc42 gene, and reported that the Cdc42-null ES cells can proliferate normally. These findings suggest a possibility that other Cdc42-related GTPases such as TC10 and Chp may compensate for the absence of Cdc42. Indeed, the mitotic phenotype in Cdc42 RNAi cells appear milder than that found in toxin B–treated cells. Recently, we found that RNAi for all of the five Cdc42-related GTPases induces a more dramatic phenotype than that of RNAi for Cdc42 alone (unpublished data).

An interesting question is where Cdc42 is localized and functions in mitosis. Our immunofluorescence study showed that Cdc42 localizes on the mitotic spindle of HeLa cells during prometaphase and metaphase and is concentrated in the central spindle in anaphase and in the bridge MTs in the midbody at the end of cell division. This Cdc42 localization is consistent with the reported localization of Ect2 during cell division (Tatsumoto et al., 1999). Association of these molecules with spindle MTs was also suggested by a recent proteome study of isolated midbody preparation (Skop et al., 2004). Interestingly, Ect2-N1 accumulates in the vicinity of the kinetochores of metaphase cells (Fig. 7 D). Ect2 may generate GTP-bound Cdc42 around the kinetochores of metaphase chromosomes. Together, our results provide evidence that Ect2 and MgcRacGAP regulate the activation and function of Cdc42 spatio-temporally in mitosis, the former catalyzing the guanine nucleotide exchange of Cdc42 to activate Cdc42 in metaphase, and the latter facilitating the GTP hydrolysis of Cdc42 in prometaphase.

Materials and methods

Materials

Rabbit polyclonal antibody, P-1 to Cdc42 and C-20 to Ect2, and mouse mAb, B-8 to Cdc42 and 26C4 to RhoA, were purchased from Santa Cruz Biotechnology, Inc. Mouse mAb 05–389 to Rac1 and Tub 2.1 to β-tubulin were purchased from Upstate Biotechnology and Sigma-Aldrich, respectively. CREST serum recognizing CENP-A was provided by T. Mimori (Kyoto University, Kyoto, Japan). Polyclonal antibody to MgcRacGAP and cDNA for MgcRacGAP^{R386A} were reported previously (Hirose et al., 2001). All other materials used were of reagent grade.

Plasmids, siRNA preparation, and transfection

pGEX4T1-CRIB-Pak has been described previously (Matsuo et al., 2002). Ect2 cDNA was provided by T. Miki (National Institutes of Health, Bethesda, MD). pCEV32F-Ect2-N1 has been described previously (Kimura et al., 2000). pEGFP-Ect2-N1 was generated by digestion of pCEV32F-Ect2-N1 with BamHI and EcoRI and inserted into BglII–EcoRI–digested pEGFP-C1. pEGFP-EB1, pEGFP-histone H2Bk, pEGFP-Cdc42^{G12V}, and pDsRed2-histone H2Bk have been described previously (Yasuda et al., 2004).

To generate siRNA against Ect2 and Cdc42, we used the BLOCK-iT RNAi-TOPO Transcription and the BLOCK-iT Dicer RNAi kits (Invitrogen). In brief, the NH_2-terminal 1,000 nucleotides of Ect2, starting from the first methionine, were amplified by PCR using the primers ATGGCTGAAAATAGTGTATTAACATCCACT and ATTTCTTGAGCTCAGGAGTATTTGCCTTTT. The full coding sequence of Cdc42 (G25K, *Homo sapiens*) was amplified by using the primers ATGCAGACAATTAAGTGTGTTGTTGTGGGCGA and TCATAGCAGCACACACCTGCGGGCTCTTCTT. The PCR fragments obtained were linked to the T7 promoter and amplified again by PCR. The T7-linked PCR products were used for transcription of single stranded RNA and subsequently annealed with complementary RNA to obtain double stranded RNA. As control RNAi, we used RNA duplex for the *Escherichia coli* LacZ gene as provided by the manufacturer. The RNA duplexes obtained were cleaved into 21–23 nucleotide fragments with Dicer enzyme.

Transfection was performed using Lipofectamine-Plus Reagent (Invitrogen). A total of 1 or 4 μg of plasmid DNA was used to transfect HeLa cells in a well of a 6-well plate or a 10-cm dish, respectively. To transfect siRNA into HeLa cells, we used Lipofectamine 2000 (Invitrogen). For immunofluorescence, we used 0.3 μg of siRNA together with 0.5 μg of pEGFP-histone H2B and 6 μl of Lipofectamine 2000 diluted in Opti-MEM. The mixture was added to one well of a 6-well plate and incubated for 2 h at 37°C with 5% CO_2. For time-lapse imaging, the cells were transfected with pEGFP-EB1 and pDsRed2-histone H2Bk, together with 0.3 μg of siRNA for either Ect2 or Cdc42 or both. The medium was replaced by DME containing 10% FCS and allowed to incubate for 48 h before observation.

Cell culture and synchronization

HeLa S3 cells were maintained in DME supplemented with 10% FCS and antibiotics at 37°C and with 5% CO_2. Cells were synchronized at early S phase by the double thymidine block as described previously (Bostock et al., 1971). In brief, cells were seeded at a density of 2×10^5 per dish onto 10-cm dishes. After overnight culture, the medium was replaced by

DME containing 10 mM thymidine and 5% FCS, and the cells were incubated for 12 h. The thymidine-containing medium was removed and the cells were washed twice with PBS without divalent cations. The cells were further cultured in DME containing 10% FCS for 10 h, and then subjected to the second thymidine block for 12 h. The cells were washed twice with PBS and placed in fresh DME containing 10% FCS. Cells were collected in G2 phase, prometaphase, metaphase, telophase, and G1 phase as described previously (Kimura et al., 2000). The cells were either frozen immediately for pull-down assays or used for immunofluorescence. In overexpression experiments, we prolonged the time of the second thymidine block to 15 h, during which we transfected cells using Lipofectamine Plus, 8 to 11 h after the addition of thymidine. For cell cycle analysis, we cotransfected cells with siRNA and pEGFP-histone H2Bk, stained the cells with propidium iodide, and subsequently examined the progression of cells expressing EGFP-histone H2Bk by flow cytometry (Darzynkiewicz, 1994).

Pull-down assays

Recombinant GST-Pak-CRIB was prepared and conjugated with glutathione-Sepharose 4B (Amersham Biosciences) as described previously (Matsuo et al., 2002). Frozen HeLa S3 cells were suspended in the lysis buffer containing 50 mM Tris-HCl, pH 7.5, 100 mM NaCl, 2 mM $MgCl_2$, 1% NP-40, and 10% glycerol supplemented with 10 mM NaF, 1 mM $NoVO_4$, 100 μg/ml PMSF, 5 μg/ml leupeptin, and 5 μg/ml pepstatin. The cell suspension was incubated for 15 min at 4°C with continuous agitation and centrifuged at 18,000 *g* for 15 min at 4°C. Supernatant was saved and sonicated on ice for 1 s 10 times. Protein concentration was determined by the Lowry method, and 800 μg of the supernatant protein was incubated with 40 μg of GST-CRIB-Pak for 30 min at 4°C. The beads were spun down and washed three times with the lysis buffer. One fourth or one eighth of the precipitates were subjected to SDS-PAGE to determine the amounts of GTP-Rac and GTP-Cdc42, respectively, and one twenty fifth of the supernatant was used to determine the total amounts of Rac and Cdc42. Separated proteins were transferred onto nitrocellulose membranes (Schleicher & Schuell; BA 83). The membranes were blotted with antibodies to Cdc42 (P-1) and Rac1. After the density of each band was determined, the amount of GTP-Cdc42 was calculated by (the density of each GTP-Cdc42 band × 8)/(the density of the total Cdc42 band in the G2 phase of each blot × 25), and expressed as a percentage of the total amount. The amount of GTP-Rac was calculated similarly. The pull-down assay for RhoA was performed as described previously (Kimura et al., 2000).

Time-lapse live imaging

HeLa cells were seeded on 35-mm glass-bottomed dishes (MatTek) and after overnight culture the cells were transfected with pEGFP-EB1 and pDsRed2-histone H2Bk, together with siRNA of Ect2 or Cdc42 or both, as described in the section Plasmids, siRNA preparation, and transfection. After 48 h, the dish was placed on a temperature-controlled stage maintained at 37°C with 5% CO_2. Live-imaging was performed on an inverted microscope (model DMIRE2; Leica) with 63× NA 1.3 lenses equipped with a high pressure lamp (Xenon). EGFP, DsRed, and brightfield images were taken with a camera (model CoolSNAP HQ) driven by AS MDW software (Leica). Sequential time-lapse images were acquired every 2.5 min for control RNAi or at 5-min intervals for Ect2 and Cdc42 RNAi. For the cells shown in Fig. 4 (A and B), one Z section was recorded at each time interval. For the cell shown in Fig. 4 C, a collection of 20 Z sections at 0.5-μm step intervals were acquired. The images obtained from Fig. 4 (B and C) were processed by deconvolution using a nonblind method and analyzed with AS MDW and Deblur software (Leica).

Immunofluorescence

Cells collected at various times of mitosis were washed with PBS before fixation with 3.7% PFA in PBS at 37°C for 15 min. The cells were washed three times with PBS and permeabilized with 0.5% Triton X-100 in PBS for 5 min, followed by three washes with PBS. For kinetochore and Mad2 staining, the cells were preextracted with 0.5% Triton X-100 in PHEM buffer (60 mM Pipes, 25 mM Hepes, 10 mM EGTA, and 1 mM Mg-acetate, pH 6.9) for 1 min on ice just before fixation with 3.7% PFA in PBS (Dujardin et al., 1998). After immersion in 100 mM glycine in PBS for 30 min, samples were incubated with 3% BSA in PBS for 30 min. The samples were incubated for 1 h at RT or 4°C overnight with indicated combinations of the following primary antibodies: anti–β-tubulin (1:200), anti-Mad2 (Covance; 1:100), and CREST serum (1:500). After three washes with PBS, the samples were incubated with appropriate secondary antibodies coupled to Alexa Fluor 488, Alexa Fluor 594, or Alexa Fluor 647 (Molecular Probes) and DAPI (WAKO). The samples were washed three times with PBS before mounting on glass slides. For detection of Cdc42, cells on the coverslips were rinsed with PHEM solution and extracted with 0.5% Triton X-100 in PHEM for 1 min before fixation with 3.7% PFA in PBS at RT. Antibodies to Cdc42 and MgcRacGAP were used at 1:200 and 1:1,000 dilution, respectively. Immunofluorescence for mDia3 has been described previously (Yasuda et al., 2004).

For high-resolution imaging, fluorescence images were obtained with a microscope (model IX70; Olympus) using oil immersion objective lenses (PlanApo 60, NA 1.4; and PlanApo 100, NA 1.4) and high-selectivity filters under the control of softWoRx software. Serial optical section data (15–30 focal planes at 0.5-μm intervals for 60× or 0.2-μm intervals for 100× objectives) were collected on a Peltier-cooled charge-coupled device (Photometrics) and computationally processed by a three-dimensional deconvolution method (Agard et al., 1989).

Online supplemental material

Fig. S1 shows the mitotic phenotype of HeLa cells expressing CRIB-Pak. Videos 1–3 show mitosis of HeLa cells transfected with control siRNA, Ect2 siRNA, and Cdc42 siRNA, respectively. Online supplemental material is available at http://www.jcb.org/cgi/content/full/jcb.200408085/DC1.

We thank J. Monypenny for critical reading of the manuscript; A. Fujita, N. Watanabe, T. Furuyashiki, and T. Ishizaki for discussion; S. Tsukita for use of a DeltaVision system; M. Yanagida for helpful advice; K. Nonomura for technical assistance; and T. Arai, H. Nose, and Y. Kitagawa for secretarial assistance.

F. Oceguera-Yanez was a recipient of the Monbukagakushou scholarship. This work was supported by grants from a Grant-in-Aid for Specially Promoted Research to S. Narumiya and a Grant-in-Aid for Scientific Research (B) to T. Haraguchi and Y. Hiraoka from the Ministry of Education, Culture, Sports, Science and Technology of Japan; a grant from the Ministry of Health, Labor and Welfare of Japan; and a Core Research for Evolutionary Science and Technology grant from the Japan Science and Technology Agency to T. Haraguchi and Y. Hiraoka.

Submitted: 13 August 2004
Accepted: 18 November 2004

References

Agard, D.A., Y. Hiraoka, P. Shaw, and J.W. Sedat. 1989. Fluorescence microscopy in three dimensions. *Methods Cell Biol.* 30:353–377.

Agnel, M., L. Roder, C. Vola, and R. Griffin-Shea. 1992. A *Drosophila* rotund transcript expressed during spermatogenesis and imaginal disc morphogenesis encodes a protein which is similar to human Rac GTPase-activating (racGAP) proteins. *Mol. Cell. Biol.* 12:5111–5122.

Aktories, K., G. Schmidt, and I. Just. 2000. Rho GTPases as targets of bacterial protein toxins. *Biol. Chem.* 381:421–426.

Ban, R., Y. Irino, K. Fukami, and H. Tanaka. 2004. Human mitotic spindle-associated protein PRC1 inhibits MgcRacGAP activity toward Cdc42 during the metaphase. *J. Biol. Chem.* 279:16394–16402.

Bostock, C.J., D.M. Prescott, and J.B. Kirkpatrick. 1971. An evaluation of the double thymidine block for synchronizing mammalian cells at the G1-S border. *Exp. Cell Res.* 68:163–168.

Chen, F., L. Ma, M.C. Parrini, X. Mao, M. Lopez, C. Wu, P.W. Marks, L. Davidson, D.J. Kwiatkowski, T. Kirchhausen, et al. 2000. Cdc42 is required for PIP(2)-induced actin polymerization and early development but not for cell viability. *Curr. Biol.* 10:758–765.

Cleveland, D.W., Y. Mao, and K.F. Sullivan. 2003. Centromeres and kinetochores: from epigenetics to mitotic checkpoint signaling. *Cell.* 112:407–421.

Darzynkiewicz, Z. 1994. Cell cycle analysis by flow cytometry. *In* Cell Biology: A Laboratory Handbook. Vol. 1. J.E. Celis, editor. Academic Press, New York. 261–271.

Dujardin, D., U.I. Wacker, A. Moreau, T.A. Schroer, J.E. Rickard, and J.R. De Mey. 1998. Evidence for a role of CLIP-170 in the establishment of metaphase chromosome alignment. *J. Cell Biol.* 141:849–862.

Etienne-Manneville, S., and A. Hall. 2001. Integrin-mediated activation of Cdc42 controls cell polarity in migrating astrocytes through PKCζ. *Cell.* 106:489–498.

Etienne-Manneville, S., and A. Hall. 2002. Rho GTPases in cell biology. *Nature.* 420:629–635.

Hirose, K., T. Kawashima, I. Iwamoto, T. Nosaka, and T. Kitamura. 2001. MgcRacGAP is involved in cytokinesis through associating with mitotic spindle and midbody. *J. Biol. Chem.* 276:5821–5828.

Jantsch-Plunger, V., P. Gönczy, A. Romano, H. Schnabel, D. Hamill, R. Schnabel, A.A. Hyman, and M. Glotzer. 2000. CYK-4: A Rho family GTPase activating protein (GAP) required for central spindle formation and cytokinesis. *J. Cell Biol.* 149:1391–1404.

Kawashima, T., K. Hirose, T. Satoh, A. Kaneko, Y. Ikeda, Y. Kaziro, T. Nosaka, and T. Kitamura. 2000. MgcRacGAP is involved in the control of growth and differentiation of hematopoietic cells. *Blood.* 96:2116–2124.

Kimura, K., T. Tsuji, Y. Takada, T. Miki, and S. Narumiya. 2000. Accumulation of GTP-bound RhoA during cytokinesis and a critical role of ECT2 in this accumulation. *J. Biol. Chem.* 275:17233–17236.

Kishi, K., T. Sasaki, S. Kuroda, T. Itoh, and Y. Takai. 1993. Regulation of cytoplasmic division of *Xenopus* embryo by rho p21 and its inhibitory GDP/GTP exchange protein (rho GDI). *J. Cell Biol.* 120:1187–1195.

Li, F., L. Adam, R.K. Vadlamudi, H. Zhou, S. Sen, J. Chernoff, M. Mandal, and R. Kumar. 2002. p21-activated kinase 1 interacts with and phosphorylates histone H3 in breast cancer cells. *EMBO Rep.* 3:767–773.

Mabuchi, I., Y. Hamaguchi, H. Fujimoto, N. Morii, M. Mishima, and S. Narumiya. 1993. A rho-like protein is involved in the organisation of the contractile ring in dividing sand dollar eggs. *Zygote.* 1:325–331.

Matsuo, N., M. Hoshino, M. Yoshizawa, and Y. Nabeshima. 2002. Characterization of STEF, a guanine nucleotide exchange factor for Rac1, required for neurite growth. *J. Biol. Chem.* 277:2860–2868.

Miki, T., C.L. Smith, J.E. Long, A. Eva, and T.P. Fleming. 1993. Oncogene ect2 is related to regulators of small GTP-binding proteins. *Nature.* 362:462–465.

Minoshima, Y., T. Kawashima, K. Hirose, Y. Tonozuka, A. Kawajiri, Y.C. Bao, X. Deng, M. Tatsuka, S. Narumiya, W.S. May Jr., et al. 2003. Phosphorylation by Aurora B converts MgcRacGAP to a RhoGAP during cytokinesis. *Dev. Cell.* 4:549–560.

Moon, S.Y., and Y. Zheng. 2003. Rho GTPase-activating proteins in cell regulation. *Trends Cell Biol.* 13:13–22.

Prokopenko, S.N., A. Brumby, L. O'Keefe, L. Prior, Y. He, R. Saint and H.J. Bellen. 1999. A putative exchange factor for Rho1 GTPase is required for initiation of cytokinesis in *Drosophila*. *Genes Dev.* 13:2301–2314.

Skop, A.R., H. Liu, J. Yates III, B.J. Meyer, and R. Heald. 2004. Dissection of the mammalian midbody proteome reveals conserved cytokinesis mechanisms. *Science.* 305:61–66.

Somers, W.G., and R. Saint. 2003. A RhoGEF and Rho family GTPase-activating protein complex links the contractile ring to cortical microtubules at the onset of cytokinesis. *Dev. Cell.* 4:29–39.

Tatsumoto, T., X. Xie, R. Blumenthal, I. Okamoto, and T. Miki. 1999. Human ECT2 is an exchange factor for Rho GTPases, phosphorylated in G2/M phases, and involved in cytokinesis. *J. Cell Biol.* 147:921–928.

Tatsumoto, T., H. Sakata, M. Dasso, and T. Miki. 2003. Potential roles of the nucleotide exchange factor ECT2 and Cdc42 GTPase in spindle assembly in *Xenopus* egg cell-free extracts. *J. Cell. Biochem.* 90:892–900.

Toure, A., O. Dorseuil, L. Morin, P. Timmons, B. Jegou, L. Reibel, and G. Gacon. 1998. MgcRacGAP, a new human GTPase-activating protein for Rac and Cdc42 similar to *Drosophila* rotundRacGAP gene product, is expressed in male germ cells. *J. Biol. Chem.* 273:6019–6023.

Vadlamudi, R.K., L. Adam, R.A. Wang, M. Mandal, D. Nguyen, A. Sahin, J. Chernoff, M.C. Hung, and R. Kumar. 2000. Regulatable expression of p21-activated kinase-1 promotes anchorage-independent growth and abnormal organization of mitotic spindles in human epithelial breast cancer cells. *J. Biol. Chem.* 275:36238–36244.

Van de Putte, T., A. Zwijsen, O. Lonnoy, V. Rybin, M. Cozijnsen, A. Francis, V. Baekelandt, C.A. Kozak, M. Zerial, and D. Huylebroeck. 2001. Mice with a homozygous gene trap vector insertion in mgcRacGAP die during pre-implantation development. *Mech. Dev.* 102:33–44.

Wang, Y.L. 2001. The mechanism of cytokinesis: reconsideration and reconciliation. *Cell Struct. Funct.* 26:633–638.

Wittmann, T., A. Hyman, and A. Desai. 2001. The spindle: a dynamic assembly of microtubules and motors. *Nat. Cell Biol.* 3:E28–E34.

Yasuda, S., F. Oceguera-Yanez, T. Kato, M. Okamoto, S. Yonemura, Y. Terada, T. Ishizaki, and S. Narumiya. 2004. Cdc42 and mDia3 regulate microtubule attachment to kinetochores. *Nature.* 428:767–771.

Yu, X., C.C.S. Chini, M. He, G. Mer, and J. Chen. 2003. The BRCT domain is a phospho-protein binding domain. *Science.* 302:639–642.

Zheng, Y. 2001. Dbl family guanine nucleotide exchange factors. *Trends Biochem. Sci.* 26:724–732.

THE JOURNAL OF CELL BIOLOGY

ROCK-I regulates closure of the eyelids and ventral body wall by inducing assembly of actomyosin bundles

Yoshihiko Shimizu,[1,2] Dean Thumkeo,[1] Jeongsin Keel,[1] Toshimasa Ishizaki,[1] Hiroko Oshima,[1] Masanobu Oshima,[1] Yoichi Noda,[2] Fumio Matsumura,[3] Makoto M. Taketo,[1] and Shuh Narumiya[1]

[1]Department of Pharmacology, Kyoto University Faculty of Medicine, Sakyo-ku, Kyoto 606-8501, Japan
[2]Department of Obstetrics and Gynecology, Shiga University of Medical Science, Ohtsu, Shiga 520-2191, Japan
[3]Department of Molecular Biology and Biochemistry, Rutgers University, Piscataway, NJ 08855

Rho-associated kinase (ROCK) I mediates signaling from Rho to the actin cytoskeleton. To investigate the in vivo functions of ROCK-I, we generated ROCK-I–deficient mice. Loss of ROCK-I resulted in failure of eyelid closure and closure of the ventral body wall, which gave rise to the eyes open at birth and omphalocele phenotypes in neonates. Most ROCK-I$^{-/-}$ mice died soon after birth as a result of cannibalization of the omphalocele by the mother. Actin cables that encircle the eye in the epithelial cells of the eyelid were disorganized and accumulation of filamentous actin at the umbilical ring was impaired, with loss of phosphorylation of the myosin regulatory light chain (MLC) at both sites, in ROCK-I$^{-/-}$ embryos. Stress fiber formation and MLC phosphorylation induced by EGF were also attenuated in primary keratinocytes from ROCK-I$^{-/-}$ mice. These results suggest that ROCK-I regulates closure of the eyelids and ventral body wall through organization of actomyosin bundles.

Introduction

The small GTPase Rho contributes to cellular functions such as cell motility, adhesion, and cytokinesis through reorganization of the actin cytoskeleton. Rho is activated by extracellular signals such as lysophosphatidic acid as well as during progression of the cell cycle. Rho activation results in assembly of contractile actin–myosin bundles, which include stress fibers in interphase cells and the contractile ring in dividing cells (Narumiya, 1996; Etienne-Manneville and Hall, 2002). The actions of Rho are mediated by downstream Rho effectors, a variety of which have been identified on the basis of their selective interaction with the active form of Rho. One such effector is Rho-associated kinase (ROCK), which includes ROCK-I (also known as ROK β) and ROCK-II (also known as Rho-kinase or ROK α; Riento and Ridley, 2003). ROCK mediates Rho signaling and reorganizes the actin cytoskeleton through phosphorylation of several substrates that contribute to the assembly of actin filaments and contractility. For example, ROCK phosphorylates both the myosin regulatory light chain (MLC) and myosin phosphatase, thereby regulating the level of MLC phosphorylation both directly and indirectly (Amano et al., 2000). Phosphorylation of MLC induces smooth muscle contraction as well as the formation of both stress fibers and focal adhesions. ROCK also phosphorylates and activates LIM-kinase, which in turn phosphorylates the cofilin/actin-depolymerizing factor complex and thereby inhibits its ability to mediate depolymerization and severing of actin filaments (Maekawa et al., 1999).

Elucidation of the roles of ROCK in the intact mammalian body has been facilitated by the introduction of a specific ROCK inhibitor, Y-27632 (Uehata et al., 1997). Studies with this inhibitor have revealed that ROCK regulates various physiological and pathological processes including smooth muscle contraction associated with hypertension and asthma, and cell migration associated with inflammation and tumor metastasis. However, relatively little is known of the role of ROCK in development. In addition, given that Y-27632 inhibits the activity of both ROCK-I and ROCK-II, studies with this inhibitor provide limited information on the specific functions of each ROCK isoform. To explore such specific functions of ROCK-I and ROCK-II, we have generated mice deficient in these enzymes individually. We previously described the generation and phenotype of ROCK-II knockout mice (Thumkeo et al., 2003). Most

Y. Shimizu and D. Thumkeo contributed equally to this work.

J. Keel was deceased on 6 September 2000.

Correspondence to Shuh Narumiya: snaru@mfour.med.kyoto-u.ac.jp

Abbreviations used in this paper: α-SMA, α-smooth muscle actin; dpc, d postcoitum; EGFR, EGF receptor; EOB, eyes open at birth; JNK, c-Jun NH_2-terminal kinase; MLC, myosin regulatory light chain; ROCK, Rho-associated kinase.

The Journal of Cell Biology, Vol. 168, No. 6, March 14, 2005 941–953
http://www.jcb.org/cgi/doi/10.1083/jcb.200411179

ROCK-II–deficient embryos manifest extensive thrombus formation in the placenta, resulting in placental dysfunction, intrauterine growth retardation, and fetal death. These animals thus revealed an important role for ROCK-II in placental homeostasis during the perinatal period.

Closure and subsequent reopening of the eyelids are common to all mammals during development. In mice, eyelid closure occurs between 15.5 and 16.5 d postcoitum (dpc), when the outermost epithelial layer of the eyelid rim extends toward the center to cover the entire ocular surface and fuses with the opposite eyelid epithelium. The eyelids are tightly closed at birth and remain so until 12 d after birth, with complete separation occurring 1 or 2 d later (Findlater et al., 1993; Kaufman, 2002). Mutations of several genes cause the eyes open at birth (EOB) phenotype. Implication of EGF receptor (EGFR) signaling in the eyelid closure and its similarity to dorsal closure in *Drosophila* are discussed (Martin and Parkhurst, 2004; Xia and Karin, 2004).

Another example of tissue closure during mammalian development is closure of the ventral body wall. At midgestation, visceral organs rapidly expand in volume and exceed the space of the peritoneal cavity, resulting in protrusion of the midgut loop from this cavity through the umbilical ring. This "physiological umbilical hernia" is first apparent at 10.5 dpc in mice. At 15.5 dpc, the midgut loop begins to return to the peritoneal cavity, and by 16.5 dpc the physiological umbilical hernia has disappeared with closure of the umbilical ring and resorption of the space formerly occupied by the gut within the umbilical cord (Kaufman, 2002). Failure of umbilical ring closure results in omphalocele, in which organs such as the liver and gut protrude from the peritoneal cavity.

We now show that ROCK-I knockout mice exhibit both EOB and omphalocele phenotypes as a result of disorganization of actomyosin cables in the eyelid epithelium and defective actin assembly in the umbilical ring.

Results

Targeted disruption of the mouse ROCK-I gene

We disrupted the ROCK-I gene by replacing exons 3 and 4, which encode part of the kinase domain, with genes for β-galactosidase and neomycin resistance (Fig. 1 A). Chimeric mice were generated, and males were mated with C57BL/6N females to produce heterozygous ROCK-I$^{+/-}$ mice, which were then intercrossed. The genotypes of offspring were determined by Southern blot analysis and PCR with DNA obtained from the tail (Fig. 1, B and C). Loss of ROCK-I protein was confirmed by immunoblot analysis (Fig. 1 D). A 160-kD protein corresponding to ROCK-I was detected in the adult brain of wild-type mice but not in that of ROCK-I$^{-/-}$ mice. In contrast, the abundance of ROCK-II did not differ between the two genotypes, indicating that the expression of ROCK-II did not increase to compensate for the loss of ROCK-I. We made use of the *lacZ* reporter gene inserted in-frame with the initiator methionine codon of ROCK-I in the targeting construct to examine the pattern of ROCK-I gene expression by whole-mount staining of ROCK-I$^{-/-}$ embryos for β-galactosidase activity with the substrate X-Gal. Such staining was detected in many locations throughout the embryo, including the skin, heart, aorta, umbilical blood vessels, and dorsal root ganglia (Fig. 1 E).

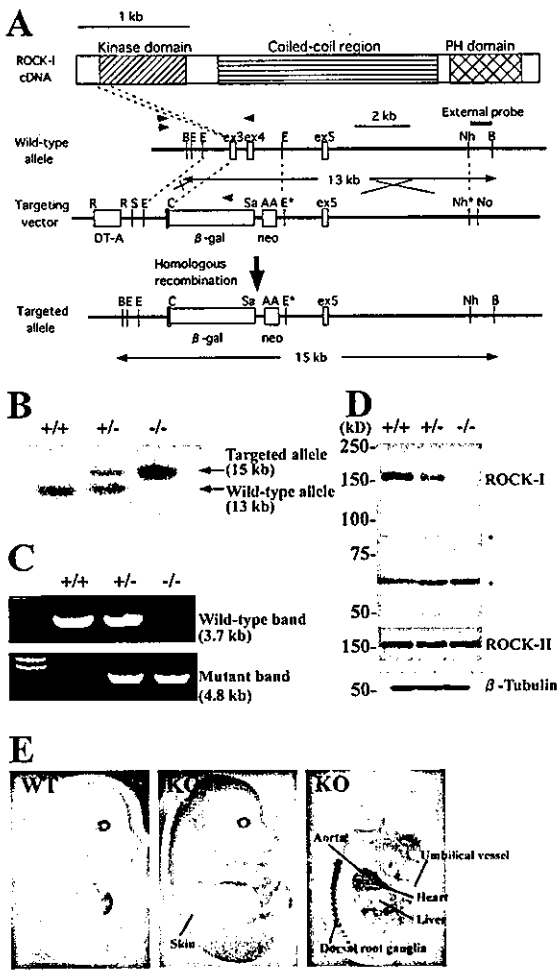

Figure 1. **Generation of ROCK-I–deficient mice.** (A) Schematic representations of the domain structure of mouse ROCK-I cDNA, the wild-type ROCK-I allele, the targeting vector, and the targeted allele. Positions of β-galactosidase (β-gal), neomycin resistance (neo), and diphtheria toxin A (DT-A) genes; of restriction sites for BglII (B), EcoRV (E), NheI (Nh), RsrII (R), SmaI (S), ClaI (C), SalI (Sa), AscI (A), and NotI (No); and of exons 3 (ex3), 4, and 5 are shown. The restriction sites indicated by asterisks are lost due to blunt-end ligation. Positions of primers for PCR analysis are indicated by arrowheads. The external probe is a unique 3′ genomic probe that distinguishes the 13-kb wild-type BglII fragment from the 15-kb BglII fragment generated by the targeted allele. (B) Southern blot analysis of genomic DNA obtained from mouse tail. The genotypes of the wild-type, heterozygous, and homozygous knockout mice are shown as +/+, +/−, and −/−, respectively. (C) Genotyping by PCR analysis of genomic DNA from mouse tail. The leftmost lane contains molecular size standards. (D) Immunoblot analysis of whole-brain lysates of adult ROCK-I$^{+/+}$, ROCK-I$^{+/-}$, and ROCK-I$^{-/-}$ mice with antibodies specific for either ROCK-I, ROCK-II, or β-tubulin. Positions of molecular mass markers are shown on the left. Asterisks indicate nonspecific bands. (E) X-Gal staining of wild-type (WT) and ROCK-I$^{-/-}$ (KO) embryos at 15.5 dpc (left and middle) or 13.5 dpc (right, sagittal section). X-Gal staining was detected in the skin, heart, aorta, umbilical blood vessels, and dorsal root ganglia of ROCK-I$^{-/-}$ embryos.

Table I. Genotypes of offspring obtained by crossing of ROCK-I$^{+/-}$ mice

Stage	Total no. of offspring	No. of mice of each genotype		
		+/+	+/-	-/-
14.5 dpc	40	12	20	8
15.5 dpc	145	40	73	32
16.5 dpc	56	14	28	14
18.5 dpc	344	86	168	90
4 wk	316	101	203	12

EOB and omphalocele phenotypes of ROCK-I-deficient mice

Analysis of genotype distribution in offspring from heterozygote crosses revealed that the homozygous mutant mice were present in the expected Mendelian ratio during embryonic development at all stages including 18.5 dpc. However, the ROCK-I$^{-/-}$ mice were greatly underrepresented among littermates at 4 wk old (Table I).

Examination of embryos at 18.5 dpc revealed EOB and omphalocele phenotypes that were fully penetrant in ROCK-I$^{-/-}$ mice (Fig. 2 A). At this stage of development, wild-type mice manifest fused eyelids and resolution of the physiological umbilical hernia. There was no substantial difference between wild-type and ROCK-I$^{+/-}$ littermates in this regard (unpublished data). Different degrees of fusion impairment were apparent in the eyelids of ROCK-I$^{-/-}$ mice; 50% (17/34) of such embryos had fully open eyelids, whereas the eyelids of the remaining 50% (17/34) of embryos were almost fully fused but manifested a hole with a diameter of <1 mm (Fig. 2 B). Some of the surviving ROCK-I$^{-/-}$ mice gradually developed apparent proliferative inflammation of the eyelid that almost covered the entire eye; this phenotype was observed in 50% (6/12) of ROCK-I$^{-/-}$ mice at 5–6 mo old (Fig. 2 C). This eye lesion may result from secondary effects due to the open state of the eye in neonates.

Omphalocele was apparent also in varying degrees and was classified into three types (Fig. 2 A): severe omphalocele, including the liver and small intestine (9/34, 26.5%); moderate omphalocele, with only the small intestine protruding (13/34, 38.2%); and mild omphalocele, in which the intestine protrudes upon crying (12/34, 35.3%). There was no correlation between the extent of EOB and that of omphalocele. The presence of an omphalocele does not affect survival in utero, and we found that the loss of ROCK-I$^{-/-}$ mice occurred immediately after birth. The umbilicus was not closed and intraperitoneal bleeding was evident in the dead ROCK-I$^{-/-}$ neonates (Fig. 2 D). We further noted that parts of several visceral organs, notably the liver and intestine, had been gnawed at in mutant neonates (Fig. 2, E and F). Because we confirmed that visceral organs were fully intact in 18.5 dpc mutant (not depicted), these results indicate that the mother had cannibalized the omphalocele together with the protruded organs in the process of clearing

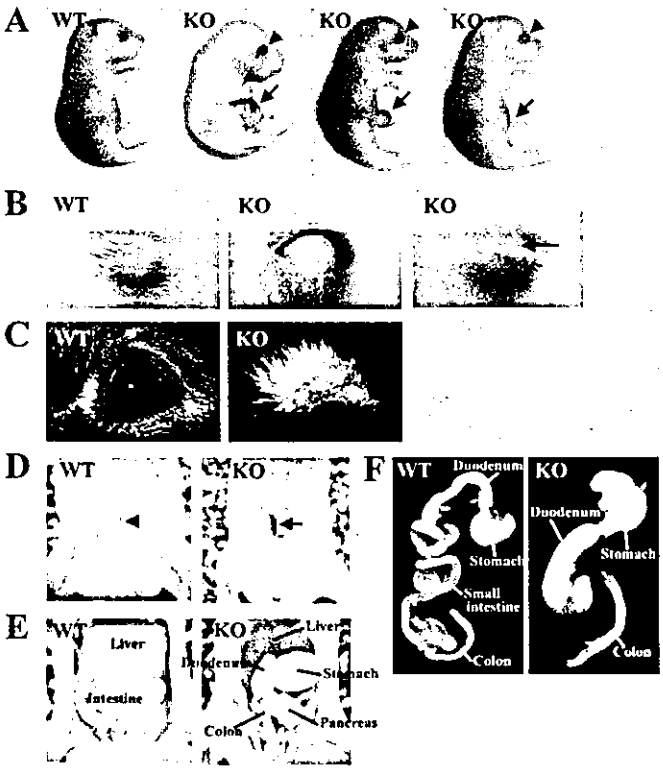

Figure 2. **EOB and omphalocele phenotypes of ROCK-I-deficient mice.** (A) Wild-type and ROCK-I$^{-/-}$ embryos at 18.5 dpc. Arrowheads and arrows indicate EOB and omphalocele phenotypes, respectively. Severe, moderate, and mild forms of omphalocele in the mutant embryos are shown from left to right. (B) Eyes of wild-type and ROCK-I$^{-/-}$ mice at 18.5 dpc. The eyes of the ROCK-I$^{-/-}$ embryos are either fully open (middle) or partially open (right; arrow indicates a small hole). (C) Eyes of adult wild-type and ROCK-I$^{-/-}$ mice. (D) Umbilical region of wild-type and ROCK-I$^{-/-}$ neonates. The umbilical ring in the wild-type neonate is closed (arrowhead), whereas that in the ROCK-I$^{-/-}$ neonate remains open (arrow). (E) Visceral organs in the abdominal cavity of the neonates shown in D. The ventral body wall was removed to render the visceral organs visible. Portions of the liver and intestine are absent in the ROCK-I$^{-/-}$ neonate. (F) Gastrointestinal tract from the stomach to the colon of the neonates shown in D and E. A part of the small intestine is absent in the ROCK-I$^{-/-}$ mouse.

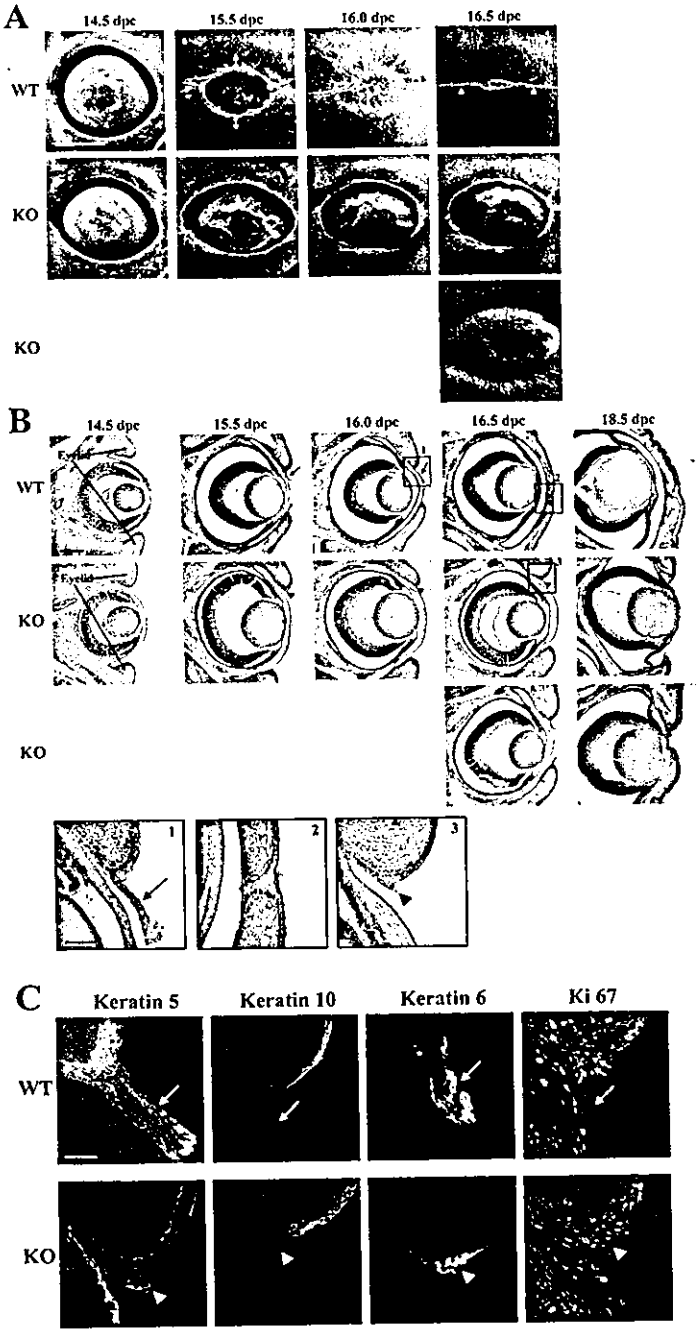

Figure 3. **Impaired eyelid closure in ROCK-I$^{-/-}$ embryos.** (A) Scanning electron micrographs of the eyes of wild-type (top) and ROCK-I$^{-/-}$ (middle and bottom) embryos from 14.5 to 16.5 dpc. Bidirectional arrows indicate extension of the eyelid rim. Arrowheads indicate eyelid fusion in the wild-type embryos. Bar, 500 μm. (B) Hematoxylin-eosin staining of transverse eye sections from wild-type and ROCK-I$^{-/-}$ embryos from 14.5 to 18.5 dpc. Arrows indicate the eyelid epithelial sheet extending from the rim of the eyelid in the wild-type embryos. Eyelid epithelial extension was impaired in mutant embryos, with arrowheads indicating the cell mass at the expected site of sheet formation. Bar, 200 μm. Boxed regions 1–3 are also shown enlarged. Bar, 20 μm. (C) Immunofluorescence staining (green) for keratins 5, 10, and 6 as well as for Ki67 in frozen sections of the eyelids of wild-type or ROCK-I$^{-/-}$ embryos at 16.0 dpc. Nuclei are stained blue. Large arrows indicate the eyelid epithelial sheet; arrowheads indicate the epithelial cell mass. The two small arrows indicate the base of the eyelid epithelial sheet. Bar, 50 μm.

the placenta and umbilicus, causing the death of these neonates. Most ROCK-I$^{-/-}$ neonates therefore do not survive, leaving only a small proportion to grow to adulthood.

Most of the surviving ROCK-I$^{-/-}$ mice, both male and female, subsequently developed normally, with the exception of the eye lesions described above, and the adult mutant animals were fertile and apparently healthy. Two adult ROCK-I$^{-/-}$ mice were killed and tissue sections were stained with hematoxylin-eosin. No obvious abnormality was observed in the brain, spinal cord, heart, aorta, lung, trachea, kidney, or bladder; in endocrine organs such as the thyroid, pituitary, and adrenal glands; in hematopoietic or lymphoid organs such as bone mar-